Single cell RNA sequencing analysis of mouse cochlear supporting cell transcriptomes with activated ERBB2 receptor, a candidate mediator of hearing restoration mechanisms.

Dorota Piekna-Przybylska[1], Daxiang Na[1], Jingyuan Zhang[2], Cameron Baker[3], John M. Ashton[3], Patricia M. White[1]

[1]Department of Neuroscience, University of Rochester School of Medicine and Dentistry, Rochester, NY 14642, USA; [2]Department of Otolaryngology, Boston Children's Hospital, Boston, MA 02115, USA; [3]Genomic Research Center, University of Rochester School of Medicine and Dentistry, Rochester, NY 14642, USA

ABSTRACT

Hearing loss is generally caused by loss of the hair cells (HCs) in the organ of Corti due to noise trauma or ototoxic medications. While in birds, amphibians, and reptiles HCs are regenerated from supporting cells (SCs), mammals show only limited regenerative capacity at the neonatal stage, which quickly declines with age. One potential approach to restore hearing is to enforce regeneration of HCs through induction of cellular signaling pathways in SCs that promote dedifferentiation and proliferation. In a previous study, we showed that the constitutive activation of ERBB2 signaling in cochlear supporting cells indirectly promoted supporting cell differentiation to hair cells, both *in vivo* and *in vitro*. In the current study, we aimed at identifying mechanisms and molecular pathways activated in supporting cells with constitutive ERBB2 signaling. To this end, we used single cell RNA sequencing (scRNA-seq) to characterize the transcriptomes of individual neonatal mouse cochlear SCs that were induced to express ERBB2. We found that induction of ERBB2 *in vivo* resulted in generation of a new distinct cluster of cells with unique transcriptome. This population has de novo expression of two members of the small integrin-binding ligand n-linked glycoproteins (SIBLING) family and their regulators. We confirm expression of the SIBLING Secreted phosphoprotein 1 (SPP1) as one of the most up-regulated genes in response to ERBB2 activation. SPP1 mediates signaling through the CD44 receptor, promoting survival, proliferation, and differentiation of osteoblast lineage cells. Histological analyses of cochlear samples collected from young adult mice confirmed that induction of ERBB2 after noise exposure resulted in up-regulation of both SPP1 and its receptor CD44, and the formation of mitotic sensory stem-like cell aggregates in the organ of Corti. Our results suggest that ectopic activation of ERBB2-signaling in young adult mice secondarily promotes SPP1/CD44 signaling, possibly altering the microenvironment of the organ of Corti.

INTRODUCTION

Lost auditory hair cells in adult mammals cannot be regenerated and drive permanent hearing loss. Conversely, lost hair cells in birds are regenerated through the proliferation and differentiation of surrounding supporting cells, leading to the restoration of hearing. Limited regenerative capacity in the organ of Corti is also observed in newborn mammals and is associated with a pool of progenitor cells in the cochlear sensory epithelium[1, 2]. The identified progenitor cells include a subset of supporting cells in proximity to hair cells, such as lateral greater epithelial ridge (LGER), inner border cells (IBC), inner pillar cells (IPC), and a third-row

Deiter cells (DC)[3, 4]. Studies focusing on signaling pathways in postnatal mice that drive HC regeneration indicate that HC can regenerate through mitotic division followed by differentiation, via Wnt signal activation[3, 5, 6]. Alternatively, HC may regenerate from progenitor cells by direct trans-differentiation, which involves blocking Notch signaling[7-10]. As maturation progresses, cochlear cells become restricted from both mechanisms of regeneration[11]. This loss of capacity contrasts with vestibular tissues of the inner ear, which maintain the ability to generate limited numbers of hair cells from adult supporting cells, both *in vitro*[12] and *in vivo*[13, 14]. Similarly, stem cell-like progenitors can be isolated from adult human utricular tissue, but not cochlear tissue[15]. These findings have been interpreted to mean that even limited regeneration capacity is lost from the adult mammalian cochlea. Nonetheless, they do not rule out the possibility that quiescent adult mammalian cochlear progenitors exist, but require a different microenvironment to manifest their potential.

Hearing restoration in birds occurs regardless of the age: therefore, avians are a useful model for studying molecular pathways involved in hair cell regeneration. Early studies showed that signaling through phosphoinositide 3-kinase (PI3K) and the epidermal growth factor receptor (EGFR) family are required for inner ear supporting cell proliferation in both chicken and neonatal mice[16, 17]. Other studies on avian regeneration have implicated VEGF activation, which also signals through PI3K[18, 19]. In the EGFR family, there are four closely related receptor tyrosine kinases: ERBB1 (EGFR), ERBB2 (HER2/NEU), ERBB3 (HER3), and ERBB4 (HER4). These form homo or heterodimers with each other upon binding of the ligand and inducing molecular pathways supporting cells proliferation, migration and survival. We previously showed that constitutive activation of ERBB2, which is the preferred heterodimerization partner for the other three EGFR family members, drives proliferation of supporting cells in explant cultures in addition to supernumerary hair cell-like formation *in vivo* in the neonatal mouse cochlea[20]. Notably, in those studies, lineage tracing revealed that CA-ERBB2+ cells induced these activities in neighboring cells, suggesting the presence of an amplifying signal cascade that recruits adjacent tissue. Consistent with this interpretation, SOX2 protein was broadly down-regulated in the apical turn harboring sparse CA-ERBB2+ cells[20]. In a companion paper, we use the same transgenic mouse model to demonstrate that activation of the ERBB2-mediated signaling in supporting cells in young adult mice after traumatic noise damage correlates with partial low-frequency auditory recovery[21].

To identify ERBB2-mediated signaling pathways associated with the changes in SCs that may facilitate HC regeneration, we performed single cell RNA sequencing on sorted neonatal SCs with and without activated constitutively active (CA) ERBB2. We performed cluster-specific gene analysis to identify differentially expressed genes (DEGs) in different cell populations. Our goals were to assign clusters and DEGs to SC subtypes and identify candidate secondary signaling pathways that could act downstream of CA-ERBB2 to promote local changes. We further sought to confirm if selected downstream mediators were also expressed in the cochlea of young adult mice after damage and CA-ERBB2 activation, and if so, where they were located.

RESULTS

Experimental design to determine transcriptome profile of cochlear supporting cells expressing ERBB2.

To perform scRNA-seq analysis of SCs expressing ERBB2, we have employed the same genetic mouse model that revealed an indirect effect of ERBB2 activation on the formation of ectopic hair cell-like cells[20]. These mice harbor a mutated *ErbB2* transgene encoding a constitutively active ERBB2 protein (CA-ERBB2), which does not require ligand binding or heterodimerization with other ERBB partners for active signaling. In order to limit induction of CA-ERBB2 activation to supporting cells, we used an inducible DNA Cre recombinase under control of the supporting cell gene promoter *Fgfr3*[22]. Double heterozygotic mice harboring both an inducible "Tet-On" *CA-ErbB2* and an *Fgfr3-iCre* transgene (Supplementary Fig. 1a) were bred to homozygous line harboring a "floxed" TA transcription factor, with an IRES-GFP to use as a lineage marker ("ROSA-rtTA-GFP"). The resulting pups were genotyped to identify mice with *CA-ErbB2* and *Fgfr3-iCre* genes (denoted here as "CA-ERBB2"). Pups harboring *Fgfr3-iCre* were used as "Control". Activation of iCRE was performed by two injections of tamoxifen at P0 and P1, which resulted in activation of GFP expression to label supporting cells (Supplementary Fig. 1b, Supplementary Fig. 2a). Induction of CA-ERBB2 expression was performed at P2 by doxycycline injection. The organs of Corti were dissected from P3 pups, and GFP+ supporting cells were purified by fluorescence-activated cell sorting (FACS) (Supplementary Fig. 2b). On average, we obtained 55±13 GFP+ cells per cochleae. RNA cDNA libraries were prepared and sequenced from about 300 GFP+ single cells per genotype collected in three independent FACS experiments.

New populations of transcriptionally distinct cochlear cells arise in response to ERBB2 signaling.

Quality control metrics presented in Figure 1a reveal comparable distributions for CA-ERBB2 and Control GFP+ cells. A mean of 5,500 unique mRNA transcripts were recorded per cell, with no differences between genotypes. These transcripts were derived from sequencing libraries generated from the individual cells, which averaged 2-1/2 million counts per cell for both genotypes. Lastly, 85% of sorted cells from each genotype were identified after sorting as intact cells with less than 10% mitochondrial representation.

Unbiased clustering was used to group GFP+ cells prior to assessment of transcriptome changes associated with CA-ERBB2 expression. Based on the pattern of gene expression, FACS-purified GFP+ cells can be grouped into at least 5 clusters (Fig. 1b). Two clusters showed significant differences between Control and CA-ERBB2 samples in distribution of cochlear cells: cluster C4 is mostly comprised of Control cells, whereas cluster C3 is formed entirely by CA-ERBB2 cells (Fig. 1b, right panel). Significant changes in the cell distribution are also observed within cluster C2, where CA-ERBB2 cells have clearly segregated away from Control cells. There are no differences between Control and CA-ERBB2 in distribution of cochlear cells in clusters C0 and C1 (Fig. 1b, middle panel). Together these results suggest heterogeneity in the responses of SCs to intrinsic ERBB2 activation. In a minority of GFP+ cells, ERBB2 activation drove a

greater transcriptional response, one that differentiated the activated cells away from the parent population.

To better understand the transcriptional diversity of cochlear SC with induced ERBB2 signaling, we performed unbiased clustering that resulted in distinguishing subpopulations within clusters C0, C1 and C2. Ten unique clusters (S0-S9) were generated with two clusters composed of CA-ERBB2 cells only (Fig. 1c). Notably, in addition to cluster S4 that corresponds to C3 in first unbiased clustering, CA-ERBB2 cells in cluster C2 were distinguished as cluster S7. Most of remaining cells in cluster C2 are Control cells (~80%) and are identified as cluster S2. Another cluster represented mostly by Control cells (~90%) is S5, which corresponds to C4 in the first unbiased clustering. In remaining clusters, there is similar distribution of Control and CA-ERBB2 cochlear cells, although S8 and S9 are represented by small numbers of cells.

Assignment of SC subtypes to clusters.

To determine what type of cochlear cells are grouped in each cluster, we analyzed expression of genes used as markers identifying particular type of cochlear cells (Supplementary Table 1, Supplementary Fig. 3). At birth, *Fgfr3-iCre* can be expressed in Deiter cells (DC), inner and outer pillar cells (IPC, OPC), outer hair cells (OHC), and Hensen cells (HeC). In our system, *Fgfr3-iCre* expression is sparser, and expression in HC, DC, and HeC is biased towards the apical region (Supplementary Fig. 2), where cells are less differentiated. To assess which SCs contributed to which clusters, we graphed expression of genes specific to SC subtypes, as described for scRNA-seq of P1 SCs[23]. Here we used the 5-cluster analysis, as we anticipated a similar number of cell types. Results in Figure 2 show that the HC markers *Ccer2*, *Pvalb*, and *Insm1* are clustered together in a subset of C2 (Fig. 2b,c). The HeC marker *Fst* is expressed in C1, whereas *Nupr1* is present in both C1 & C2 (Fig. 2b,d). All five DC markers, *Hes5, Pdzk1ip1, S100a1, Prss23,* and *Lfng,* were most strongly upregulated in C2 (Fig. 2b,e). PC markers were more ambiguous, but were most up-regulated also in C2 (Fig. 2b,f). C4, which is comprised primarily of Control cells, expressed all markers examined at a moderate level and thus could not be identified. C0 is a mix of CA-ERBB2 and Control cells, and it expresses a handful of sensory-specific markers, which were *S100a1*, *S100b*, and *Cryab*. Its identity is likewise ambiguous. C3 is composed exclusively of CA-ERBB2 cells and primarily expresses OPC markers (Fig. 2b,f). However, it contains also markers identifying LGER1 (LGER group 1), such as *Dcn*, *Ddost, Pdia6, Rcn3*, and *Sdf2l1*, which are also enriched in C1 and C2.

CA-ERBB2 cochlear supporting cells are transcriptionally distinct from Control supporting cells.

Induction of ERBB2 signaling in CA-ERBB2 samples, may result in activation of genes that normally are not expressed in cochlear supporting cells. Thus, in order to identify DEGs between Control and CA-ERBB2 samples, we performed statistical analysis on the 10-cluster grouping (Fig. 1c) using both the Wilcoxon rank-sum test and the Likelihood-Ratio (LR) test. In the Wilcoxon rank-sum test, DEGs are identified among genes that have some level of expression in the compared conditions. The LR test allowed for detection of DEGs where expression is undetectable within one condition[24]. Genes were mapped in the Gene Ontology resource (geneontology.org) (Supplementary Fig. 4). Sequences that could not be mapped to a

corresponding protein record in the PANTHER classification system were designated "unmapped IDs." They mostly represent non-coding RNAs and pseudogenes.

Using Wilcoxon rank-sum, the criteria of an adjusted *p*-value of <0.05, and a difference in levels of expression greater than 2-fold, 584 DEGs were identified (Supplementary Data 1). 68 genes were up-regulated, and 516 genes were down-regulated. Around half of the genes in each group were unmapped IDs. Almost 90% of DEGs were found in less than 10% of the CA-ERBB2 population. Using the LR test approach, 1556 genes were identified as differentially expressed with an adjusted *p*-value of <0.05 and a difference in levels of expression greater than 2-fold (Supplementary Data 2). 1049 genes were up-regulated, and 507 genes were down-regulated, and around half of the genes in each group were identified as protein coding genes (Supplementary Fig. 4). About 64% of the DEGs were found in less than 10% of CA-ERBB2 population.

In both analyses, *Spp1* was among the most up-expressed genes (132-fold change) in about 80% of supporting cells with activated ERBB2 signaling, in comparison to the level of *Spp1* expression detected in 55.4% of Control cells. *Spp1* will be more fully described later. In both analyses, *Lama3* was among the most down-regulated genes in CA-ERBB2 cells. It was present in 3.4% of CA-ERBB2 cells, compared to 23.2% of Control cells. LAMA3 is a subunit of laminins, which mediate the attachment, migration and organization of cells by interacting with integrin receptors and other extracellular matrix components[25, 26]. Using LR test analysis, Kyphoscoliosis peptidase (Ky) is differentially expressed (3530-fold change), but only in about 7.3% of CA-ERBB2 cells, in comparison to 21.5% of Control cells. Ky's proposed function is maintenance of cytoskeleton and neuromuscular junction[27]. These data suggest that some CA-ERBB2+ cells modify the local environment, potentially affecting the behavior of neighboring cells. Such cells may comprise two populations of CA-ERBB2 cells (S4 & S7, Fig. 1c), which are transcriptionally distinct from Control cells.

To better understand transcriptional heterogeneity among CA-ERBB2 cells, we identified up-expressed genes in each cluster described in Figure 1c, and then examined activated pathways against the Gene Ontology (GO) biological process database. For each of 10 clusters, we analyzed gene expression in comparison to remaining clusters. Using the criteria of an adjusted *p*-value of <0.05 and a difference in levels of expression greater than 2-fold, we found 1125 genes up-expressed in cluster S0, in cluster S1 – 810 genes, S2 – 731 genes, S3 - 359 genes, S4 – 90 genes, S5 – 3722 genes, S6 – 484 genes, S7 – 1102 genes, S8 – 426 genes, and in S9 – 144 genes (Supplementary Data 3). The top 10 genes with high expression in each cell cluster were then used to generate heatmaps (Fig. 3).

The analysis revealed that among top up-expressed genes in cluster S4 are genes that were also identified as differentially expressed between CA-ERBB2 and Control samples in Wilcoxon rank-sum test (*Spp1, CD63, Tmsb4x*; Supplementary Data 1), and in the LR test (*Spp1*, *Timp1*, *Dmp1, Mmp9*, *CD63*; Supplementary Data 2). S4 was not clearly related to any other cluster. In contrast, cluster S7, comprised of CA-ERBB2 cells only, had top up-regulated DEGs in common with cluster S2, which was mostly Control cells. This indicates a close relationship and suggests that CA-ERBB2 cells in cluster S7 originated from Control cells in cluster S2. Among the top up-expressed genes of S7 are genes identified as differentially expressed between CA-ERBB2 and Control samples in the LR test (*Plet1os*, *Rufy4*, *Plet1*, *Cutal*) (Supplementary Data 2).

With respect to clusters comprised of both CA-ERBB2 and Control cells, some transcriptional relationships were also evident. For example, cluster S6 had similarities to clusters S1 and S3, which are in proximity on the UMAP analysis. In contrast, there were no marker genes up-expressed in cluster S0, and neighboring S3, although small number of cells in these clusters have up-expression of top-expressed genes found in other neighboring clusters, suggesting some transcriptional relationship. Similarly, there were no marker genes up-expressed in cluster S5, mostly composed of Control cells and separated from other clusters. Surprisingly, in cluster S5 some level of up-regulation was observed for most of the up-expressed genes identified in other clusters, with exception of up-expressed genes in cluster S8. Finally, clusters S8 and S9 are represented by small number of cells with up-expressed genes that are generally not found in other clusters, indicating that they are transcriptionally distinct populations.

CA-ERBB2 cells express genes involved in modulation of extracellular matrix.

Gene set enrichment against GO biological process was performed for up-expressed genes identified in each cluster. Results for six clusters with listed 10 top GO terms with significant *q*-value <0.05 are in Figure 4. Complete list of terms for all clusters is provided in Supplementary Data 4. Among the most enriched annotations, both by adjusted *p*-value and number of genes involved, were annotations of genes linked to extracellular matrix modulation. The distinctive cluster S4, formed entirely by CA-ERBB2 cells, showed various degrees of activation of markers involved in extracellular matrix organization (GO:0030198), and extracellular matrix disassembly (GO:0022617). Cluster S4 had also enriched genes associated with cellular response to cytokine stimulus (GO:0071345), cytokine-mediated signaling pathway (GO:0019221) and regulation of integrin-mediated signaling pathway (GO:2001044). We note that clusters S1 and S6 were also distinguished by up-expressed genes involved in extracellular matrix organization and disassembly.

With respect to the distinctive cluster S7, GO biological process analysis of up-expressed genes in CA-ERBB2 cells did not reveal terms with *q*-value <0.05. However, among terms with significant *p*-value (<0.05), are terms associated with genes *Krt17* and *Plet1* listed as differentially expressed between CA-ERBB2 and Control samples in the LR test (Supplementary Data 2). Epidermis development (GO:0008544) is associated with *Krt17* and *Col7a1* genes. This term is in a parent-child relationship with the term related to hair cell differentiation (inner ear auditory receptor cell differentiation, GO:0042491). Moreover, *Plet1* is associated with wound healing, the spreading of epidermal cells (both GO:0035313 and GO:0044319), and negative regulation of cell-matrix adhesion (GO:0001953) (Supplementary Data 4).

In the clusters S1, S2 and S6, CA-ERBB2 cells were intermingled with Control cells in the UMAP analysis suggesting that CA-ERBB2 and Control cells have similar transcriptome. However, the identified GO terms for these clusters show that cochlear cells of P3 mice still undergo changes related to development of the organ of Corti. For example, cells in cluster S1 were enriched of genes associated with transmembrane receptor protein serine/threonine kinase signaling pathway (GO:0007178), collagen fibril organization (GO:0030199), sensory organ morphogenesis (GO:0090596), regulation of endothelial cell migration (GO:0010594), endodermal cell differentiation (GO:0035987), and skeletal system development (GO:0001501). In cluster S2, cells showed up-regulation of genes involved in epithelial cell development

(GO:0002064), regulation of transcription involved in cell fate commitment (GO:0060850), and Notch signaling pathway (GO:0007219). Inspection of S2 up-regulated genes reveals multiple transcription factors involved in hair cell and supporting cell differentiation, including *Gata3*, *Isl1*, *Prox1*, *Hey1*, *Hes5*, and *Sox2*. In cluster S6, enriched genes are associated with sensory perception of mechanical stimulus (GO:0050954), and sensory perception of sound (GO:0007605).

Cells in cluster S8 were enriched of terms associated with cellular division, such as mitotic sister chromatid segregation (GO:0000070), mitotic nuclear division (GO:0140014), mitotic spindle organization (GO:0007052), microtubule cytoskeleton organization involved in mitosis (GO:1902850). Analysis of transcriptomes for cell cycle-specific gene expression confirmed that cells in cluster S8 are in S and G2/M phase (Supplementary Fig. 5). The analysis also revealed that whereas most cells across the conditions were in G1 phase, clusters S4 and S0 also showed enrichment of cells in phase S and G2/M, indicating some cells prepared for, or underwent cell division (Supplementary Fig. 5). In cluster S8, both CA-ERBB2 cells and Control cells showed markers for phase S and G2/M, however in cluster S0 this population was mostly represented by CA-ERBB2 cells.

Top up-regulated genes in cluster S4 are in close network of predicated protein-protein interactions.

We focused the next analysis on the new population of CA-ERBB2 cells that formed a transcriptionally distinct cluster S4. Top upregulated genes *Spp1, Timp1*, *Mmp9* and *Dmp1*, are found in GO annotations associated with modulation of extracellular matrix and cytokine response (Fig. 4). Using STRING software, we performed analysis of protein-protein interaction network for SPP1, TIMP1, MMP9 and DMP1. The results from a STRING search are visualized in Figure 5a, and scores for predicted interactions are summarized in Table 1. The analysis shows that interactions between SPP1, TIMP1, MMP9 and DMP1 have association scores in the high and the highest confidence range (scores above 0.7 and 0.9, respectively). Increasing the network for additional five proteins revealed CD44 as protein with close association (Fig. 5b), with the highest confidence score (above 0.9) calculated for SPP1, TIMP1, and MMP9, indicating likely true associations. Additional five proteins added to the network revealed two proteins that were found as differentially expressed between CA-ERBB2 and Control cells (Fig. 5c). These proteins were CD63 and HPX, and both have association scores in the highest confidence range (above 0.9) with TIMP1; whereas HPX has also association score in the high confidence range (above 0.7) with MMP9.

SPP1 and DMP1 are SIBLING extracellular modifiers and ligands for CD44 and integrin αvβ3 receptors, promoting survival, proliferation, differentiation, and migration[28-36]. TIMP1 is an inhibitor of MMP9, a metallopeptidase that is proposed to regulate CD44[37, 38] and also modulates NOTCH signaling[39]. The CD44 receptor is best described in the context of cancer development for its role in cell survival and proliferation, but a recent finding also highlights its important role in tissue regeneration and wound healing[32, 40-42]. Notably, CD44 is endogenously expressed on outer pillar cells in mice in adulthood[43].

Analysis of UMAP plots and split violin plots for *Spp1, Timp1*, *Mmp9* and *Dmp1* indicate that up-expression of these genes is observed in CA-ERBB2 cells in almost all clusters, with significant enrichment in cluster S4 (Fig. 5e). Some level of expression in Control cells is

detected for *Spp1* and *Timp1* genes, particularly in cluster S1, S5 and S6. For genes *Mmp9* and *Dmp1,* almost no expression is detected in Control cells, except for cluster S9 and S5. To validate the scRNA-seq analysis, we performed reverse transcriptase quantitative polymerase chain reaction (RT-qPCR) on FACS-sorted cochlear GFP+ cells collected from CA-ERBB2 and Control neonatal mice. Results of RT-qPCR analysis are shown in Figure 5f and Supplementary Figure 6 and confirm that activation of ERBB2 signaling in CA-ERBB2 cells resulted in significant up-regulated expression of genes *Spp1, Timp1*, *Mmp9* and *Dmp1,* and also other genes identified as up-expressed in CA-ERBB2 cells of cluster S4 (*Bglap*, *Bglap2*, *Ptgis*, *Cd63*, *Il12a*, *Ank*).

Induction of ERBB2 signaling in deafened adult mice results in up-regulation of *Spp1* and *Timp1*, the activation of CD44 receptor, and the formation of cellular clusters in the cochlear duct.

In order to determine if the SIBLING cluster could be induced at adult stages, we used immunostaining on sections of cochlea from adult young mice after both damage induced hearing loss and CA-ERBB2 induction. Mice harboring the *Fgfr3-iCre* and *CA-Erbb2* transgenes have been backcrossed to CBA/CaJ for at least four generations, whereas the ROSA-rtTA-GFP line is congenic on C57BL6/J (Supplementary Fig. 1). Thus, the experimental mice are hybrid CBA/C57 mice, whose noise damage characteristics are similar to a pure CBA/CaJ response[44]. Male and female young adult mice with Control and CA-ERBB2 genotype were first injected with tamoxifen to activate iCRE, which induces GFP and rTA expression in supporting cells (Fig. 6a). One week after baseline hearing tests, mice were exposed to traumatic noise as described in the Methods. A second hearing test was done at 1 day post noise exposure (1 DPN) to confirm a large threshold shift. At 3 DPN, the mice from both genotypes were randomly assigned to 2 groups, and treated with doxycycline and furosemide injections to initiate CA-ERBB2 expression; or with saline and furosemide injections to use as reference for doxycycline-related background. Furosemide increases doxycycline delivery into cochlea. Mice were euthanized at 5 DPN, and their cochlea were dissected and processed for immunostaining with antibodies specific for SPP1, TIMP1, and the intracellular domain of the CD44 receptor.

As shown in Figure 6b and 6c, SPP1 and TIMP1 were up-expressed in cochlear sections from CA-ERBB2 animals treated with DOX/FURO. The fluorescent immunoreactivity for SPP1 corresponded to cells that also showed GFP expression, including cells near OHC that correspond to DC, and cells near IHC corresponding to phalangeal cells and border cells. Similarly, TIMP1 was detected in cells that expressed GFP, although in sections from Control animals the immunoreactivity for TIMP1 was evident also in cells corresponding to inner phalangeal cells and border cells. Staining for the CD44 intracellular domain showed clearly up-regulation of CD44 signaling in GFP positive cells from CA-ERBB2 animals treated with DOX/FURO. In CA-ERBB2 mice, CD44 immunoreactivity was also observed in interphalangeal cells and DC, suggesting up-regulation. Interestingly, CD44 activation was also evident in cells that correspond to Hensen cells or Claudius cells, which showed the immunoreactivity also in sections from Control animals. This is consistent with previous report describing the CD44 expression to increase in postnatal mice by P7 in the outer pillar cells, Claudius cells and in a small number of GER cells[43].

Additional mice treated with traumatic noise, EdU, doxycycline and furosemide were euthanized at 7 DPN, and analyzed for GFP expression and additional markers (Fig. 7). Here we found that aggregated GFP+ and GFP-negative cells were located in the endolymphatic duct of CA-ERBB2 cochlea. Phosphorylation of ERBB2 was seen in scattered cells, and did not precisely map onto GFP expression as observed at earlier time points[20]. Mitotic figures labeled with EdU were evident in these aggregates (Fig. 7b'), as were scattered cells labeled with activated CASP3 (Fig. 7c'). Scattered cells within aggregates expressed sensory markers, including MYO7 and the supporting cell marker TAK1. They were largely absent of SOX2 and PVALB expression. Some aggregates had smooth, compacted multicellular regions that stained brightly for phalloidin. Aggregates were observed in three out of four cochleae with CA-ERBB2 induction analyzed at 72 hours after DOX injections. In Control cochleae, only single cells were observed, none of which expressed GFP.

DISCUSSION

Our studies focused on identifying candidate signals downstream of ERBB2 activation in mouse cochlear supporting cells. In a previous study, we found that supporting cells with activated ERBB2 influenced gene expression in their neighbors, suggesting that ERBB2 may initiate a signaling cascade. Single cell transcriptome analysis revealed formation of new population among a subset of cells with activated ERBB2 signaling that significantly differentiated from the parental Control cells. Possibly derived from outer pillar cells, these cells are also enriched for genes specific for lateral greater epithelial ridge cells. The population also contains most of the cells that express *Spp1*, identified in our studies as one of the most activated genes in response to ERBB2 activation. Importantly, in the new cluster formed by CA-ERBB2 cells, other three top upregulated genes, *Mmp9*, *Timp1* and *Dmp1*, together with *Spp1* are associated with the same signaling network involving CD44 and integrin αvβ3 receptors. Gene ontology enrichment analysis revealed that these genes are involved in modulation of the extracellular matrix and cytokine response. We confirmed that SPP1, TIMP1 and CD44 protein are also upregulated in adult cochlear supporting cells after CA-ERBB2 induction. We also observed a later formation of floating aggregates of cochlear sensory cells. The fate and potential of these cellular aggregates are not known.

SPP1 and DMP1 are secreted glycoproteins that act as ligands for CD44 and integrin αvβ3 receptors. They are members of the small integrin-binding ligand n-linked glycoproteins (SIBLING) family. SPP1 promotes survival, proliferation, differentiation, adhesion, and migration of numerous cell types[28-34, 36]. In contrast, DMP1 function in injury and wound healing has not been yet determined, but it is significantly up-regulated in a number of cancerous tissues[45, 46]. SPP1 may function in the neuronal differentiation of auditory neurons during inner ear development[47]. SPP1 is detected in membranous labyrinth of the adult mammalian cochleae, particularly in the utricle, where it is currently used as a marker of type I hair cells[48-51]. Generally, SPP1 is not expressed in the organ of Corti, although RNA-seq analysis of individually collected cochlear cells from adult mice detected low levels of *Spp1* transcripts in pillar cells and Deiter cells[52].

The most significant aspect of up-regulation of SPP1, MMP9 and TIMP1 in response to ERBB2 signaling, is that they promote wound healing and regeneration after injury in other systems[32, 40-42]. SPP1 is well known to mediate bone and muscle regeneration[53-57], and it is also

involved in promoting proliferation and regeneration in nervous system[58-60]. In recent studies, Want et al. demonstrated that binding of SPP1 with CD44 and integrin αvβ3 is important in the Schwann cells function in regenerating nerves, by promoting proliferation and survival after peripheral nerve injury[61]. Another study by Powell and colleagues showed that SPP1 together with MMP9 acts through CD44 receptor to mediate synaptogenesis after central nervous system (CNS) insult[62]. The mechanism of SPP1 and MMP9 interactions with CD44 receptor is unknown, and it may differ depending on the variant form of CD44 receptor. Interestingly, *in vitro* SPP1 has been shown to be a substrate of MMP9 cleavage, which exposes the N terminal fragment of SPP1 that is known to interact with CD44 and integrin αvβ3 receptors[63, 64].

TIMP1 is an inhibitor of MMP9 and the balance between them is a key regulator of the signaling network in the injured nerve[42]. The significance of MMP9/TIMP1 balance is not well understood, but it was also demonstrated to regulate healing process of burned fetal skin[65]. An increased MMP9/TIMP1 ratio promotes the degradation of extracellular matrix (ECM) to allow cellular migration, while a reduced MMP9/TIMP1 ratio drives reconstruction of the ECM during healing process[65]. TIMP1 may also act as cytokine independently of MMP9 inhibition to promote cell survival and proliferation[66]. In hematopoietic stem and progenitor cells, TIMP1 promotes migration, adhesion and survival by binding to CD63-integrin β1 receptors complex[67]. Our scRNA-seq analysis revealed CD63 as differentially expressed gene and its up-regulation was mostly enriched in cluster S4 formed by CA-ERBB2 cells (Supplementary Data 1 and 2). Other receptors involved in the MMP9-independend TIMP-1-induced cell proliferation are still unknown.

Up-regulation of SPP1, MMP9, TIMP1 and DMP1 in response to ERBB2 activation suggests that its downstream signaling involves CD44 receptor and potentially also integrin receptors. The relationship between ERBB2 and CD44 was previously described for maintaining neuron–Schwann cell interactions in early rat neonatal nerves development[68]. In particular, CD44 significantly enhanced neuregulin-induced ERBB2 phosphorylation and ERBB2–ERBB3 heterodimerization, and was found to coimmunoprecipitates with ERBB2 and ERBB3, indicating that CD44 constitutively associates with each receptor[68]. The CD44-ERBB2 interactions were also described for human ovarian tumor cell[69]. Importance of CD44 receptor's network in cells survival, proliferation and regeneration described for Schwann cell and in other tissues, suggests that some of CA-ERBB2 effects involve signaling through CD44 receptor.

Lower flexibility of the epithelium associated with cell-cell junction was proposed as one of the mechanisms responsible for decreased regenerative capacity of the adult mammalian cochlea[70]. Our results indicate that activation of ERBB2 signaling promotes modulation of extracellular matrix that would allow increased flexibility in the organ of Corti. The combination of EGF and GSK3 inhibitors were recently reported to deplete E-cadherin in tight junctions of the adult mammalian cochlea[71]. In addition to up-regulated genes in cluster S4 and also cluster S1, that are associated with extracellular matrix disassembly, there is also up-regulated *Plet1* gene in CA-ERBB2 cells from cluster S7, which is associated with negative regulation of cell-matrix adhesion (GO:0001953). Its up-regulation in CA-ERBB2 cells would allow for increased local movements of cells. The protein is also listed in GO terms associated with wound healing, and spreading of cells (GO:0044319, GO:0035313).

Importance of ERBB2-mediated ECM modulation for hair cells regeneration is also supported by recent studies indicating that extracellular matrix and integrin receptors are

induced in early neurosensory development and cell fate determination in the human fetal inner ear[72]. We speculate that enforced activation of signaling pathways through ERBB family receptors might allow for changes in the environment of the organ of Corti that promote the proliferation of supporting cells and permit the regeneration of hair cells. Previous studies have shown little or no stem cell activity in the adult mammalian cochlea[15, 73]. This contrasts to robust stem-like capacity in isolated cells from the adult utricle[12, 15], which correlates with limited regeneration potential in that organ[13]. These data may be interpreted to mean that cochlear stem cells, perhaps resident in the greater epithelial ridge[74], are lost during maturation. It is also possible that their requirements for survival or for identity maintenance differ. For example, they may require accessory cells to maintain their microenvironmental niche. Alternatively, the forced expression of CA-ERBB2 signaling might promote novel behaviors not otherwise seen in cochlear supporting cells.

In conclusion, we report that enforced signaling of ERBB2 in a minority of cochlear supporting cells, possibly outer pillar cells, drives a novel differentiation response in the neonatal mouse cochlea. These cells induce expression of a cluster of genes involved in signaling, wound healing, and migration. We confirm that at least two of these genes, SPP1 and CD44, are also upregulated in adult cochlear cells after CA-ERBB2 induction. CA-ERBB2 induction also correlates with the generation of cellular aggregates in the cochlear duct. These aggregates contain, but are not limited to, fate-mapped CA-ERBB2 cells. Their potential, effects, and fate remain to be determined.

METHODS

Ethical Approval

All experiments using animals were approved in advance by the University Committee on Animal Research (UCAR) at the University of Rochester, protocol number 2010-011, PI Patricia White.

Mice

The following mouse strains were used. Fgfr3-iCre[22] was a kind gift from Dr. Jian Zuo. TetON-CA-ErbB2[75] and CBA/CaJ, were purchased from Jackson Laboratories. ROSA-floxed-rtTA/GFP[76] was a kind gift from Dr. Lin Gan. Fgfr3-iCre and TetON-CA-ERBB2 mice were crosses to generate double heterozygous transgenic mice that were subsequently used as breeders. In a second breeding, double heterozygous were crossed with homozygous ROSA-floxed-rtTA/GFP mice. For scRNA-seq experiments and data validation by RT-qPCR, generated pups were genotyped at P0 to identify triple-transgenic mice that harbor *Fgfr3-iCre*, ROSA-floxed-rtTA/GFP, and TetON-CAERBB2 (named here as CA-ERBB2). Oligonucleotides used in genotyping are provided in Supplementary Table 2. Littermates with *Fgfr3-iCre* and ROSA-floxed-rtTA/GFP were used as Controls. For scRNA-seq data validation in young adults exposed to noise, both male and female mice were used equally. Three weeks old mice were genotyped and weaned, and tamoxifen injections (75 mg/kg) were performed at P21, P22 and P23. At P28 their hearing was tested by auditory brainstem response (ABR) and distortion product acoustic emissions (DPOAE)[21]. The mice were then divided into DOX exposed and control conditions.

Mice experienced a noise exposure of 110 dB of 8-16 kHz octave band noise for 2 hours, as described previously[21]. The next day (1 DPN), mice received hearing tests to confirm severe noise-induced hearing loss evident by threshold shift for about 25 dB across five frequencies (8, 12, 16, 24 and 32 kHz). Two days later (3 DPN), the DOX group were injected with DOX (100 mg/kg), followed 30 minutes later by an injection of FURO (400 mg/kg). FURO is necessary to open up tight junctions in the mouse ear and enable the penetration of the cochlear barrier by water soluble DOX[77]. The control group received a saline injection, followed by furosemide. Two days after these injections (5 DPN), the mice were euthanized and their cochleae fixed overnight in fresh 4% paraformaldehyde. The cochleae were subsequently decalcified in 100 mM EDTA in a saline solution at 4°C for 3 days. For cryosectioning, tissues were immersed in 30% sucrose in PBS overnight, embedded in OCT, frozen in liquid nitrogen, and cryosectioned at 20 microns. Sections were mounted on slide glass and kept at −30°C until use.

Cell dissociation and FACS sorting

The iCRE activity was induced by tamoxifen injections (75 mg/kg) at P0/P1 to label supporting cells with GFP and rtTA. Doxycycline injections (100 mg/kg) were performed at P2 to drive CA-ERBB2 expression in GFP+ supporting cells. Cochlea from P3 pups were collected and incubated with 1 mL Accutase® solution (Innovative Cell Technologies) for 15 minutes at 37°C. To ensure a reproducible digestion, 2-4 cochlea were treated per tube. The Accutase solution was removed and cochlea were gentle washes in ice cold Ca2+, Mg2+ - free HBSS buffer. Organs in each tube were dissociated by trituration for 2-3 minutes. Cells were then filtered with a 40 µm cell strainer (BD Biosciences) and kept on ice until sorted. For the exclusion of dead cells and debris from the samples during sorting, a single-cell suspension was stained with DAPI. Sorting was performed at 4°C in a FACSAria II cell sorter (BD Biosciences) using a 130 µm nozzle. Scatter discrimination was used to eliminate doublets and samples were negatively selected with DAPI to remove dead cells and debris. For scRNA-seq, single GFP+ cells were captured into 96-well plate with 11.5 µl lysis buffer and RNase Inhibitor without the CDS IIA Oligo (Takara Bio, Mountain View, CA), and stored at -80°C until used for construction of cDNA libraries. On average, 6 pups per genotype were processed for sorting single GFP+ cells into one 96-well plate. For data validation by RT-qPCR, GFP+ cells were captured into single tube with 100 µl lysis buffer containing Proteinase K and DNase (Bio-Rad). The sorted cells were then incubated for 10 min. in room temperature, followed by 5 min. at 37°C, and 5 min. at 75°C. The samples were stored at -80°C until RT-qPCR analysis.

Construction of single-cell RNA-seq libraries

Single-cell RNA-seq libraries were constructed according to the SMART-Seq Single PLUS protocol (Takara Bio, Mountain View, CA). Frozen plates were thawed on ice. Next, cDNA was generated with the addition of the 3' SMART-Seq CDS Primer II A and SMARTScribe II RT reagents. cDNA was amplified via 20 cycles of PCR, purified, and assessed for quantity and quality by Qubit dsDNA assay (ThermoFisher, Waltham, MA) and Fragment Analyzer (Agilent, Santa Clara, CA) analysis, respectively. For each well, 1 ng amplified cDNA was fragmented and prepared for library construction with the addition of stem-loop adapters. Final library amplification and indexing was performed through 16 cycles of PCR amplification. Following

bead purification, individual library profiles were assessed by Fragment Analyzer and quantified by Qubit dsDNA assay. Libraries were diluted, pooled in equimolar amounts, and sequenced on a NovaSeq S1 flowcell (Illumina, San Diego, CA) to generate an average of 10 million reads per cell.

Data preprocessing, Seurat clustering, and visualization

Raw reads generated from the Illumina basecalls were demultiplexed using bcl2fastq version 2.19.1. Quality filtering and adapter removal are performed using FastP version 0.20.1 with the following parameters: "--length_required 35 --cut_front_window_size 1 --cut_front_mean_quality 13 --cut_front --cut_tail_window_size 1 --cut_tail_mean_quality 13 --cut_tail -y -r". Processed/cleaned reads were then mapped to the Mus musculus reference genome (GRCm38 + Gencode-M25 Annotation) using STAR_2.7.6a with the following parameters: "—twopass Mode Basic --runMode alignReads --outSAMtype BAM SortedByCoordinate – outSAMstrandField intronMotif --outFilterIntronMotifs RemoveNoncanonical –outReads UnmappedFastx". Gene level read quantification was derived using the subread-2.0.1 package (featureCounts) with a GTF annotation file (Gencode M25) and the following parameters: "-s 2 -t exon -g gene_name". The data generated by the sequencing was used to create a Seurat object using the Seurat package in R (v4.0.5 and v4.1.2). Quality control metrics were performed using standard Seurat (v4.0.4 and v4.1.0) protocols and included the identification of unique genes ("features") per cell, the total number of molecules detected ("reads"), and the percent of mitochondrial genome contamination. The data was normalized. Clusters were identified with the Louvain method, using PCA and UMAP to reduce dimensionality and plot the cells. Ten clusters were identified using a dimensionality reduction of 1:30 within the Nearest-neighbor graph construction and UMAP generation, as well as a resolution of 2 within clustering. In addition to performing sample filtering and clustering, Seurat handled differential expression to determine genes up-regulated within clusters and across condition groups. enrichR (v3.0) was used to perform gene set enrichment on DEGs[78]. A final report was rendered using Rstudio and rmarkdown (v2.10). Identity of genes was analyzed in the Gene Ontology resource (http://geneontology.org/)[78]. GO biological process analysis was performed for up-expressed genes identified in each cluster. Since there were to many up-expressed genes for some of the clusters we limited the number of markers coming from specific clusters based off of log fold change. The log fold change threshold for cluster S7 was 4, for cluster S0 was 4, and for cluster S5 was 6. The log fold change threshold for the remaining clusters remained at 2. The protein interaction network modules were visualized using STRING network online analysis (http://string-db.org)[79].

RT-qPCR analysis

Cell lysates prepared after sorting GFP+ cells into single tube were used in RT-qPCR analysis using SingleShot Two-Step RT-qPCR reagents (Bio-Rad) according to manufacture instruction. Each qPCR reaction was performed on cells lysates corresponding to 10 cells. Three technical replicates were used for each analyzed gene. Wells with primers but without cDNA sample were utilized for negative controls, while cell lysates not treated with reverse transcriptase were used as a control of genomic DNA contamination. qPCR reactions were performed using Bio-Rad CFX Thermal Cycler and the threshold of cycles (Ct) values was calculated with Bio-Rad

CFX Manager Software. ΔΔCt method was used for calculating relative gene expression. *Eef1a1* and *Tubb4a* were used as reference genes to calculate differences in gene expression between Control and CA-ERBB2 cells[80]. The Ct values of technical replicates were averaged and expression of the gene in CA-ERBB2 sample and Control sample was normalized to reference gene (REF) expression level within the same sample to determine ΔCt ($Ct_{(gene)} – Ct_{(REF)}$). For each gene, analysis of relative gene expression was performed from at least three biological samples (three independent FACS sortings). The ΔCt for each biological replicate was exponentially transformed to the ΔCt expression ($2^{-\Delta Ct}$) before averaging and determining the standard deviation (SD). The mean was then normalized to the expression of gene in Control sample to find ΔΔCt expression in CA-ERBB2 sample. Oligonucleotides used in RT-qPCR are provided in Supplementary Table 2.

Immunochemistry

Immunostaining of cryostat cochlear sections was performed to examine the expression of selected genes. The sections were permeabilized and blocked in PBS with 0.5% Triton X-100 and 5% donkey serum (TDB buffer) for 1 h at 4°C, followed by incubation with primary antibodies in TDB at 4°C overnight. The sections were rinsed briefly 4 times in PBS, then incubated with secondary antibodies in TDB at 4°C overnight. The sections were rinsed briefly 4 times in PBS. The following primary antibodies were used: chicken anti-GFP (1:100; Abcam; AB_300798), mouse anti-PVALB (1:1000, EMD Millipore; MAB1572), goat anti-OPN (1:100; R&D Systems; AF808), goat anti-TIMP1 (1:100; R&D Systems; AF980), rabbit anti-CD44 (1:100; Abcam; AB157107). Secondary antibodies were purchased from Jackson Immunoresearch. Imaging was performed using Confocal Microscope Olympus FV1000.

DATA AVAILABILITY

All data supporting the findings of this study are available within the article and its Supplementary Information files. Single-cell gene expression data have been deposited in the Gene Expression Omnibus data repository under accession code: GSE202850.

ACKNOWLEDGMENTS

We gratefully acknowledge Dr. Anne Luebke, who maintains the URMC Small Animal Auditory Testing Core; Dr. Jian Zuo for the Fgfr3-iCre mouse strain; and Dr. Lin Gan for the ROSA-floxed rtTA/GFP mouse strain. This data was supported by grants from the United States Department of Defense DOD RH190035 (P.W.), the National Institute of Health R01 DC014261 (P.W.), and the Schmitt Program of Integrative Neuroscience.

ETHICS DECLARATIONS

Competing interest

The authors declare no competing interests.

REFERENCES

1. Zhang, S.*, et al.* Hair cell regeneration from inner ear progenitors in the mammalian cochlea. *Am J Stem Cells* **9**, 25-35 (2020).
2. Atkinson, P.J., Huarcaya Najarro, E., Sayyid, Z.N. & Cheng, A.G. Sensory hair cell development and regeneration: similarities and differences. *Development* **142**, 1561-1571 (2015).
3. Shi, F., Kempfle, J.S. & Edge, A.S. Wnt-responsive Lgr5-expressing stem cells are hair cell progenitors in the cochlea. *J Neurosci* **32**, 9639-9648 (2012).
4. Chai, R.*, et al.* Dynamic expression of Lgr5, a Wnt target gene, in the developing and mature mouse cochlea. *J Assoc Res Otolaryngol* **12**, 455-469 (2011).
5. Shi, F.*, et al.* beta-Catenin is required for hair-cell differentiation in the cochlea. *J Neurosci* **34**, 6470-6479 (2014).
6. Chai, R.*, et al.* Wnt signaling induces proliferation of sensory precursors in the postnatal mouse cochlea. *Proc Natl Acad Sci U S A* **109**, 8167-8172 (2012).
7. Yamamoto, N.*, et al.* Inhibition of Notch/RBP-J signaling induces hair cell formation in neonate mouse cochleas. *J Mol Med (Berl)* **84**, 37-45 (2006).
8. Korrapati, S., Roux, I., Glowatzki, E. & Doetzlhofer, A. Notch signaling limits supporting cell plasticity in the hair cell-damaged early postnatal murine cochlea. *PLoS One* **8**, e73276 (2013).
9. Bramhall, N.F., Shi, F., Arnold, K., Hochedlinger, K. & Edge, A.S. Lgr5-positive supporting cells generate new hair cells in the postnatal cochlea. *Stem Cell Reports* **2**, 311-322 (2014).
10. Mizutari, K.*, et al.* Notch inhibition induces cochlear hair cell regeneration and recovery of hearing after acoustic trauma. *Neuron* **77**, 58-69 (2013).
11. Brown, R. & Groves, A.K. Hear, Hear for Notch: Control of Cell Fates in the Inner Ear by Notch Signaling. *Biomolecules* **10** (2020).
12. Li, H., Liu, H. & Heller, S. Pluripotent stem cells from the adult mouse inner ear. *Nat Med* **9**, 1293-1299 (2003).
13. Burns, J.C. & Stone, J.S. Development and regeneration of vestibular hair cells in mammals. *Semin Cell Dev Biol* **65**, 96-105 (2017).
14. Bucks, S.A.*, et al.* Supporting cells remove and replace sensory receptor hair cells in a balance organ of adult mice. *Elife* **6** (2017).
15. Senn, P.*, et al.* Progenitor Cells from the Adult Human Inner Ear. *Anat Rec (Hoboken)* **303**, 461-470 (2020).
16. Witte, M.C., Montcouquiol, M. & Corwin, J.T. Regeneration in avian hair cell epithelia: identification of intracellular signals required for S-phase entry. *Eur J Neurosci* **14**, 829-838 (2001).
17. White, P.M., Stone, J.S., Groves, A.K. & Segil, N. EGFR signaling is required for regenerative proliferation in the cochlea: conservation in birds and mammals. *Dev Biol* **363**, 191-200 (2012).
18. Wan, L., Lovett, M., Warchol, M.E. & Stone, J.S. Vascular endothelial growth factor is required for regeneration of auditory hair cells in the avian inner ear. *Hear Res* **385**, 107839 (2020).
19. Matsunaga, M.*, et al.* Initiation of Supporting Cell Activation for Hair Cell Regeneration in the Avian Auditory Epithelium: An Explant Culture Model. *Front Cell Neurosci* **14**, 583994 (2020).

20. Zhang, J.*, et al.* ERBB2 signaling drives supporting cell proliferation in vitro and apparent supernumerary hair cell formation in vivo in the neonatal mouse cochlea. *Eur J Neurosci* **48**, 3299-3316 (2018).
21. Zhang, J.*, et al.* ERBB2 is a Key Mediator in Hearing Restoration in Noise-Deafened Young Adult Mice. *bioRxiv* (2021).
22. Cox, B.C., Liu, Z., Lagarde, M.M. & Zuo, J. Conditional gene expression in the mouse inner ear using Cre-loxP. *J Assoc Res Otolaryngol* **13**, 295-322 (2012).
23. Kolla, L.*, et al.* Characterization of the development of the mouse cochlear epithelium at the single cell level. *Nat Commun* **11**, 2389 (2020).
24. McDavid, A.*, et al.* Data exploration, quality control and testing in single-cell qPCR-based gene expression experiments. *Bioinformatics* **29**, 461-467 (2013).
25. Belkin, A.M. & Stepp, M.A. Integrins as receptors for laminins. *Microsc Res Tech* **51**, 280-301 (2000).
26. Hamill, K.J., Paller, A.S. & Jones, J.C. Adhesion and migration, the diverse functions of the laminin alpha3 subunit. *Dermatol Clin* **28**, 79-87 (2010).
27. Hedberg-Oldfors, C.*, et al.* A new early-onset neuromuscular disorder associated with kyphoscoliosis peptidase (KY) deficiency. *Eur J Hum Genet* **24**, 1771-1777 (2016).
28. Flores, M.E., Norgard, M., Heinegard, D., Reinholt, F.P. & Andersson, G. RGD-directed attachment of isolated rat osteoclasts to osteopontin, bone sialoprotein, and fibronectin. *Exp Cell Res* **201**, 526-530 (1992).
29. Sodek, J., Ganss, B. & McKee, M.D. Osteopontin. *Crit Rev Oral Biol Med* **11**, 279-303 (2000).
30. Ashkar, S.*, et al.* Eta-1 (osteopontin): an early component of type-1 (cell-mediated) immunity. *Science* **287**, 860-864 (2000).
31. Rangaswami, H., Bulbule, A. & Kundu, G.C. Osteopontin: role in cell signaling and cancer progression. *Trends Cell Biol* **16**, 79-87 (2006).
32. Denhardt, D.T., Noda, M., O'Regan, A.W., Pavlin, D. & Berman, J.S. Osteopontin as a means to cope with environmental insults: regulation of inflammation, tissue remodeling, and cell survival. *J Clin Invest* **107**, 1055-1061 (2001).
33. Kazanecki, C.C., Uzwiak, D.J. & Denhardt, D.T. Control of osteopontin signaling and function by post-translational phosphorylation and protein folding. *J Cell Biochem* **102**, 912-924 (2007).
34. Jain, A., Karadag, A., Fohr, B., Fisher, L.W. & Fedarko, N.S. Three SIBLINGs (small integrin-binding ligand, N-linked glycoproteins) enhance factor H's cofactor activity enabling MCP-like cellular evasion of complement-mediated attack. *J Biol Chem* **277**, 13700-13708 (2002).
35. Wu, H.*, et al.* Dentin matrix protein 1 (DMP1) signals via cell surface integrin. *J Biol Chem* **286**, 29462-29469 (2011).
36. Karadag, A., Fedarko, N.S. & Fisher, L.W. Dentin matrix protein 1 enhances invasion potential of colon cancer cells by bridging matrix metalloproteinase-9 to integrins and CD44. *Cancer Res* **65**, 11545-11552 (2005).
37. Visse, R. & Nagase, H. Matrix metalloproteinases and tissue inhibitors of metalloproteinases: structure, function, and biochemistry. *Circ Res* **92**, 827-839 (2003).

38. Grunwald, B., Schoeps, B. & Kruger, A. Recognizing the Molecular Multifunctionality and Interactome of TIMP-1. *Trends Cell Biol* **29**, 6-19 (2019).
39. Garg, P.*, et al.* Matrix metalloproteinase-9 functions as a tumor suppressor in colitis-associated cancer. *Cancer Res* **70**, 792-801 (2010).
40. Michopoulou, A.*, et al.* A novel mechanism in wound healing: Laminin 332 drives MMP9/14 activity by recruiting syndecan-1 and CD44. *Matrix Biol* **94**, 1-17 (2020).
41. Kyriakides, T.R.*, et al.* Mice that lack matrix metalloproteinase-9 display delayed wound healing associated with delayed reepithelization and disordered collagen fibrillogenesis. *Matrix Biol* **28**, 65-73 (2009).
42. Kim, Y.*, et al.* The MMP-9/TIMP-1 axis controls the status of differentiation and function of myelin-forming Schwann cells in nerve regeneration. *PLoS One* **7**, e33664 (2012).
43. Hertzano, R.*, et al.* CD44 is a marker for the outer pillar cells in the early postnatal mouse inner ear. *J Assoc Res Otolaryngol* **11**, 407-418 (2010).
44. Milon, B.*, et al.* The impact of biological sex on the response to noise and otoprotective therapies against acoustic injury in mice. *Biol Sex Differ* **9**, 12 (2018).
45. Chaplet, M.*, et al.* Dentin matrix protein 1 is expressed in human lung cancer. *J Bone Miner Res* **18**, 1506-1512 (2003).
46. Fisher, L.W., Jain, A., Tayback, M. & Fedarko, N.S. Small integrin binding ligand N-linked glycoprotein gene family expression in different cancers. *Clin Cancer Res* **10**, 8501-8511 (2004).
47. Kim, H.J.*, et al.* Patterns of gene expression associated with Pten deficiency in the developing inner ear. *PLoS One* **9**, e97544 (2014).
48. Lopez, C.A.*, et al.* Osteopontin expression detected in adult cochleae and inner ear fluids. *Hear Res* **85**, 210-222 (1995).
49. Sakagami, M. Role of osteopontin in the rodent inner ear as revealed by in situ hybridization. *Med Electron Microsc* **33**, 3-10 (2000).
50. McInturff, S., Burns, J.C. & Kelley, M.W. Characterization of spatial and temporal development of Type I and Type II hair cells in the mouse utricle using new cell-type-specific markers. *Biol Open* **7** (2018).
51. Jan, T.A.*, et al.* Spatiotemporal dynamics of inner ear sensory and non-sensory cells revealed by single-cell transcriptomics. *Cell Rep* **36**, 109358 (2021).
52. Liu, H.*, et al.* Cell-Specific Transcriptome Analysis Shows That Adult Pillar and Deiters' Cells Express Genes Encoding Machinery for Specializations of Cochlear Hair Cells. *Front Mol Neurosci* **11**, 356 (2018).
53. Zhu, M.*, et al.* Osteopontin sequence modified mesoporous calcium silicate scaffolds to promote angiogenesis in bone tissue regeneration. *J Mater Chem B* **8**, 5849-5861 (2020).
54. Uaesoontrachoon, K.*, et al.* Osteopontin and skeletal muscle myoblasts: association with muscle regeneration and regulation of myoblast function in vitro. *Int J Biochem Cell Biol* **40**, 2303-2314 (2008).
55. Zanotti, S.*, et al.* Osteopontin is highly expressed in severely dystrophic muscle and seems to play a role in muscle regeneration and fibrosis. *Histopathology* **59**, 1215-1228 (2011).
56. Pagel, C.N., Wasgewatte Wijesinghe, D.K., Taghavi Esfandouni, N. & Mackie, E.J. Osteopontin, inflammation and myogenesis: influencing regeneration, fibrosis and size of skeletal muscle. *J Cell Commun Signal* **8**, 95-103 (2014).

57. Maeda, Y.*, et al.* CXCL12 and osteopontin from bone marrow-derived mesenchymal stromal cells improve muscle regeneration. *Sci Rep* **7**, 3305 (2017).
58. Ellison, J.A.*, et al.* Osteopontin and its integrin receptor alpha(v)beta3 are upregulated during formation of the glial scar after focal stroke. *Stroke* **29**, 1698-1706; discussion 1707 (1998).
59. Hedtjarn, M., Mallard, C. & Hagberg, H. Inflammatory gene profiling in the developing mouse brain after hypoxia-ischemia. *J Cereb Blood Flow Metab* **24**, 1333-1351 (2004).
60. Liu, X.*, et al.* Effect of Spp1 on nerve degeneration and regeneration after rat sciatic nerve injury. *BMC Neurosci* **18**, 30 (2017).
61. Wang, J.B.*, et al.* SPP1 promotes Schwann cell proliferation and survival through PKCalpha by binding with CD44 and alphavbeta3 after peripheral nerve injury. *Cell Biosci* **10**, 98 (2020).
62. Powell, M.A., Black, R.T., Smith, T.L., Reeves, T.M. & Phillips, L.L. Matrix Metalloproteinase 9 and Osteopontin Interact to Support Synaptogenesis in the Olfactory Bulb after Mild Traumatic Brain Injury. *J Neurotrauma* **36**, 1615-1631 (2019).
63. Lindsey, M.L., Zouein, F.A., Tian, Y., Padmanabhan Iyer, R. & de Castro Bras, L.E. Osteopontin is proteolytically processed by matrix metalloproteinase 9. *Can J Physiol Pharmacol* **93**, 879-886 (2015).
64. Scatena, M., Liaw, L. & Giachelli, C.M. Osteopontin: a multifunctional molecule regulating chronic inflammation and vascular disease. *Arterioscler Thromb Vasc Biol* **27**, 2302-2309 (2007).
65. Yu, G.*, et al.* Exogenous peripheral blood mononuclear cells affect the healing process of deepdegree burns. *Mol Med Rep* **16**, 8110-8122 (2017).
66. Ries, C. Cytokine functions of TIMP-1. *Cell Mol Life Sci* **71**, 659-672 (2014).
67. Wilk, C.M.*, et al.* The tissue inhibitor of metalloproteinases-1 improves migration and adhesion of hematopoietic stem and progenitor cells. *Exp Hematol* **41**, 823-831 e822 (2013).
68. Sherman, L.S., Rizvi, T.A., Karyala, S. & Ratner, N. CD44 enhances neuregulin signaling by Schwann cells. *J Cell Biol* **150**, 1071-1084 (2000).
69. Bourguignon, L.Y.*, et al.* Interaction between the adhesion receptor, CD44, and the oncogene product, p185HER2, promotes human ovarian tumor cell activation. *J Biol Chem* **272**, 27913-27918 (1997).
70. Burns, J.C.*, et al.* Reinforcement of cell junctions correlates with the absence of hair cell regeneration in mammals and its occurrence in birds. *J Comp Neurol* **511**, 396-414 (2008).
71. Kozlowski, M.M., Rudolf, M.A. & Corwin, J.T. EGF and a GSK3 Inhibitor Deplete Junctional E-cadherin and Stimulate Proliferation in the Mature Mammalian Ear. *J Neurosci* **40**, 2618-2632 (2020).
72. Johnson Chacko, L.*, et al.* Transcriptome-Wide Analysis Reveals a Role for Extracellular Matrix and Integrin Receptor Genes in Otic Neurosensory Differentiation from Human iPSCs. *Int J Mol Sci* **22** (2021).
73. Oshima, K.*, et al.* Differential distribution of stem cells in the auditory and vestibular organs of the inner ear. *J Assoc Res Otolaryngol* **8**, 18-31 (2007).
74. Udagawa, T.*, et al.* Lineage-tracing and translatomic analysis of damage-inducible mitotic cochlear progenitors identifies candidate genes regulating regeneration. *PLoS Biol* **19**, e3001445 (2021).

75. Xie, W., Chow, L.T., Paterson, A.J., Chin, E. & Kudlow, J.E. Conditional expression of the ErbB2 oncogene elicits reversible hyperplasia in stratified epithelia and up-regulation of TGFalpha expression in transgenic mice. *Oncogene* **18**, 3593-3607 (1999).
76. Belteki, G.*, et al.* Conditional and inducible transgene expression in mice through the combinatorial use of Cre-mediated recombination and tetracycline induction. *Nucleic Acids Res* **33**, e51 (2005).
77. Walters, B.J. & Zuo, J. A Sox10(rtTA/+) Mouse Line Allows for Inducible Gene Expression in the Auditory and Balance Organs of the Inner Ear. *J Assoc Res Otolaryngol* **16**, 331-345 (2015).
78. Xie, Z.*, et al.* Gene Set Knowledge Discovery with Enrichr. *Curr Protoc* **1**, e90 (2021).
79. Szklarczyk, D.*, et al.* The STRING database in 2021: customizable protein-protein networks, and functional characterization of user-uploaded gene/measurement sets. *Nucleic Acids Res* **49**, D605-D612 (2021).
80. Park, J.S.*, et al.* Identification of a Circadian Clock in the Inferior Colliculus and Its Dysregulation by Noise Exposure. *J Neurosci* **36**, 5509-5519 (2016).

Tables

Table 1. The combined score of interactions between pair of proteins in STRING database analysis. A minimum required interaction score of medium confidence is 0.4, for high confidence is 0.7, and for highest confidence is 0.9. Data shown only for interactions with SPP1, TIMP1, MMP9 and DMP1.

Figure legends

Figure 1. Quality control metrics of scRNA-seq dataset and unbiased clustering of cochlear SC transcriptomes from Control and CA-ERBB2 samples. **a**, Violin plots showing similar distributions observed for cells from Control and CA-ERBB2 samples in the number of detected transcripts per cell, in UMI counts per cell used in generating sequencing libraries, and in percentage of reads from mitochondrial transcripts per cell. Below, UMAP plots showing the distribution of CA-ERBB2 cells and Control cells in clusters, and percentage of mitochondrial gene (mt) expression in clusters. **b**, Initial unbiased clustering showing differences between Control cells and CA-ERBB2 cells in the number of clusters and in distribution of cells within the clusters. On right, bar graph showing proportion of Control and CA-ERBB2 cells found in each cluster. **c**, Second unbiased clustering distinguishes subpopulations within clusters C0, C1 and C2, generating ten unique clusters (S0-S9) with two clusters formed by CA-ERBB2 cells only (S4 and S7) and two clusters mostly composed of Control cells (S2 and S5). On right, bar graph showing proportion of Control and CA-ERBB2 cells found in each cluster. Statistical analyses were performed with Seurat package in R version 4.1.2.

Figure 2. UMAP plots and violin plots for marker gene transcripts identifying cochlear cells. **a**, Schematic cross-section of the cochlear duct showing the position of different cell types. IHC, inner hair cells; OHC, outer hair cells; GER, greater epithelial ridge; IBC, inner border cells; IPH, interphalangeal cells; IPC, inner pillar cells; OPC, outer pillar cells; DC, Deiter cells; HeC, Hensen cells. **b**, Cluster plot from Fig. 1b, with putative cell type designations. **c**, Three HC markers are presented: *Ccer2, Pvalb,* and *Insm1.* **d**, Two HeC markers are shown: *Fst* and *Nupr1.* **e**, The following marker genes were used to identify Deiter cells: *Hes5, Pdzk1ip1, S100a1, Prss23, Lfng*. **f**, Five markers for IPC and OPC are shown: *Cryab, Emid1, Npy, S100b*, and *Smagp*. **g**, Lateral GER cells express *Dcn, Ddost, Pdia6, Rcn3, Sdf2l1*. The most informative markers were chosen for display. Cochlear supporting cell identity associated with analyzed marker gene is indicated on UMAP plot. Expression of the HeC and OPC marker gene *Fam159b*, and the IHC marker gene *Acbd7* were not detected.

Figure 3. Heatmap depicting the top 10 genes expressed by 10 different clusters of cochlear SCs. Clusters S4 and S7 are composed of CA-ERBB2 cells only. Cells from each cluster are arrayed along the horizontal axis and genes are arrayed along vertical axis. Clusters are distinguished by the color bars.

Figure 4. GO term enrichment analyses performed using Enrichr on up-expressed genes identified in each cluster. For each cluster, bar chart shows the top 10 enriched biological process along with corresponding *p*-values (< 0.05). An asterisk (*) next to a *p*-value indicates the term also has a significant *q*-value (<0.05). The *y*-axis represents biological process, and the horizontal axis represents the number of genes, which are listed on the left side of the graph. Complete list of terms for each cluster is provided in Supplementary Data 4.

Figure 5. STRING protein-protein interaction network of four top upregulated genes in cluster S4. a. Protein-protein interaction network connectivity among SPP1, TIMP1, MMP9 and DMP1.

In (**b**) and (**c**) are shown protein-protein networks with increasing number of closely associated genes. An edge was drawn with colored lines representing a type of evidence used in predicting the associations. A purple line indicates experimental evidence; a light green line indicates text-mining evidence; a light blue line indicates database evidence; a black line indicates co-expression evidence; and a light violet line indicates protein homology. The score interactions are summarized in Table 1. In (**d**), UMAP plot with marked cluster S4 enriched in cells expressing *Spp1*, *Timp1*, *Mmp9* and *Dmp1* in response to induction of ERBB2 signaling. In (**e**), UMAP plots and split violin plots showing up-regulated expression of *Spp1*, *Timp1*, *Mmp9* and *Dmp1* in CA-ERBB2 compared to Control cells in different clusters. **f**, RT-qPCR validation of scRNA-seq analysis performed on GFP+ FACS-sorted cells from P3 cochleae. The level of gene expression in CA-ERBB2 sample is presented as ΔΔCt value (± SD) relative to Control (CTRL) normalized against the expression of the two reference genes *Eef1a1* (E) and *Tubb4a* (T) (n=3). Significance (*$p<0.05$; ** $p<0.01$) was determined by unpaired *t*-test (one-tailed) analysis.

Figure 6. SPP1 and TIMP1 together with CD44 signaling are up-regulated in cochlear cells two days after CA-ERBB2 induction in noise exposed young adults. **a**, Timeline of noise exposure (NE), GFP activation (TAM), CA-ERBB2 activation (DOX), and hearing tests (HT) in young adult mice. Mice were exposed to 110 dB octave band noise for 2 hours, and 3 days later injected with doxycycline (DOX) to induce CA-ERBB2 expression. HT were performed 1 DPN to confirm hearing loss. Immunostaining of cochlea sections revealed detection of SPP1 (**b**), and TIMP1 (**c**) together with activated CD44 receptor in CA-ERBB2 animals. Immunodetection for hair cells (PVALB, red), and cells competent to express CA-ERBB2 (GFP, green), are shown in panels 1 and 2. Immunodetection of activated CD44 receptor (blue) is shown in panels 1 and 3. Immunodetection of SPP1 and TIMP1 are shown in panel 1, 3 and 4 (gray).

Figure 7. Four days after CA-ERBB2 induction, aggregates of sensory cells can be found within the cochlear duct. Brightfield low power images are used to show the position of the cellular aggregates, while immunostaining reveals specific markers. **a** and **a'**, GFP (green) and pERBB2 (magenta) are present in an aggregate attached to the spiral limbus, which has little SOX2 (white). **b** and **b'**, A similarly localized aggregate harbors GFP+ cells (green) and rare MYO7+ cells (white), with EdU+ mitotic figures (magenta) in cells lacking GFP. **c** and **c'**, An aggregate near the stria vascularis contains GFP+ cells (green), rare apoptotic cells marked with anti-activated CASP3 (magenta), and compacted epithelial cells revealed by phalloidin staining (white). **d** and **d'**, Another aggregate near the stria vascularis harbors cells with GFP (green) and neighboring cells positive for the supporting cell marker TAK1 (magenta), but no PVALB+ hair cells.

Table 1

node 1	node 2	Combined score	node 1	node 2	Combined score
Timp1	Mmp9	0.998	Mmp14	Timp1	0.998
Dmp1	Mmp9	0.898	Mmp14	Spp1	0.443
Spp1	Timp1	0.757	Mmp3	Timp1	0.999
Dmp1	Spp1	0.74	Mmp3	Spp1	0.975
Mmp9	Spp1	0.73	Mmp3	Mmp9	0.919
Cd44	Spp1	0.998	Cd63	Timp1	0.993
Cd44	Mmp9	0.995	Cd63	Mmp9	0.473
Cd44	Timp1	0.917	Cdh1	Mmp9	0.986
Cd44	Dmp1	0.471	Cdh1	Spp1	0.582
Itgav	Spp1	0.998	Cdh1	Timp1	0.552
Itgav	Dmp1	0.852	Hpx	Timp1	0.99
Itgav	Mmp9	0.581	Hpx	Mmp9	0.756
Itgb1	Spp1	0.996	Lcn2	Mmp9	0.993
Itgb1	Timp1	0.845	Lcn2	Timp1	0.686
Itgb1	Mmp9	0.815	Lcn2	Spp1	0.55
Itgb1	Dmp1	0.448	Timp3	Mmp9	0.991

Figure 1

a

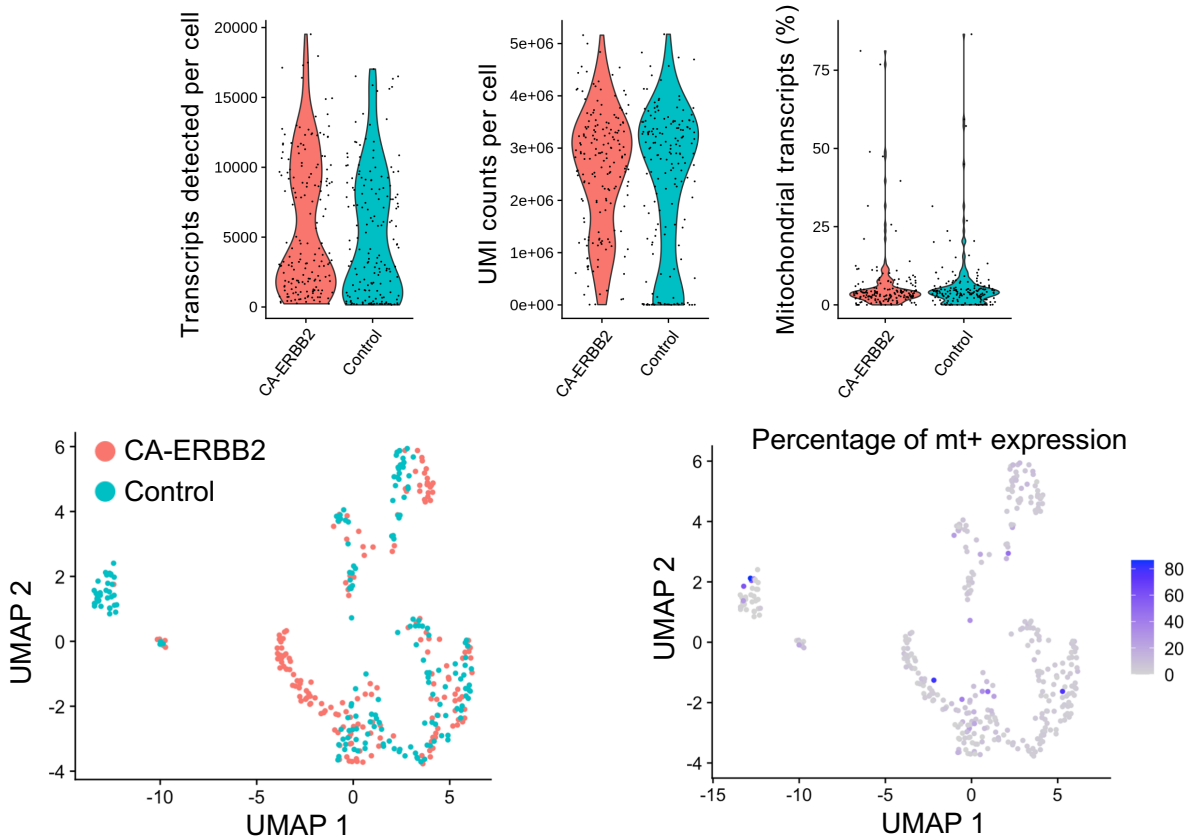
Transcripts detected per cell
UMI counts per cell
Mitochondrial transcripts (%)
CA-ERBB2
Control
CA-ERBB2
Control
Percentage of mt+ expression
UMAP 1
UMAP 2

b

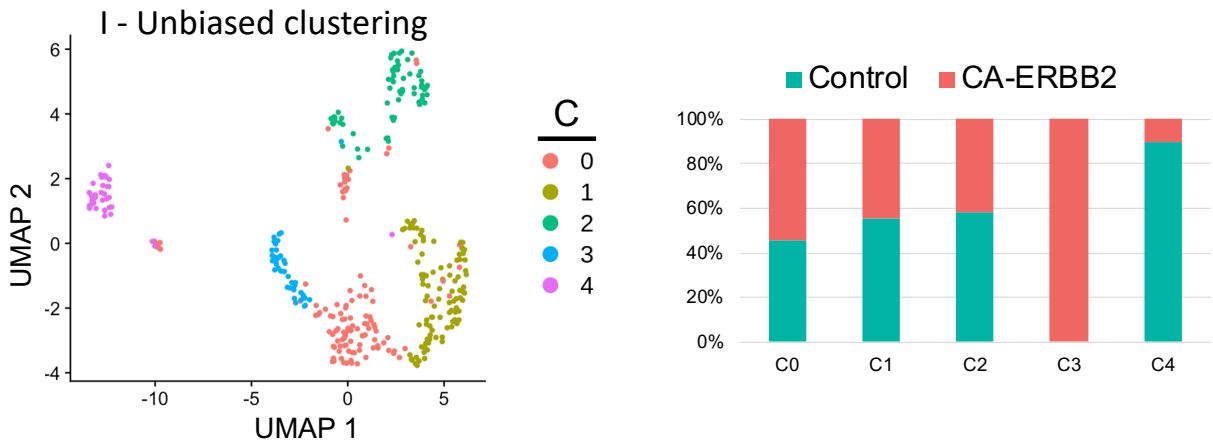
I - Unbiased clustering
UMAP 1
UMAP 2
C
0
1
2
3
4
Control
CA-ERBB2
C0
C1
C2
C3
C4

c

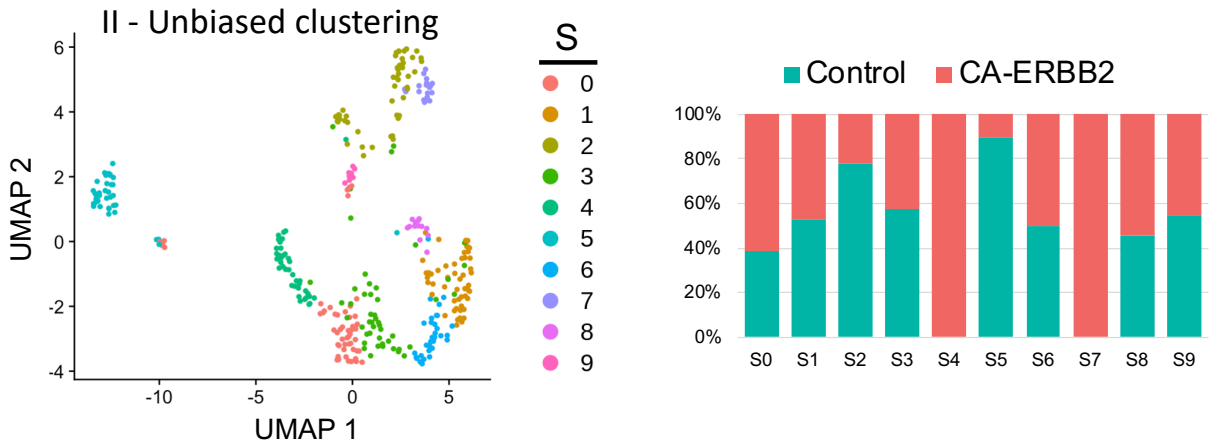
II - Unbiased clustering
UMAP 1
UMAP 2
S
0
1
2
3
4
5
6
7
8
9
Control
CA-ERBB2
S0
S1
S2
S3
S4
S5
S6
S7
S8
S9

Figure 2

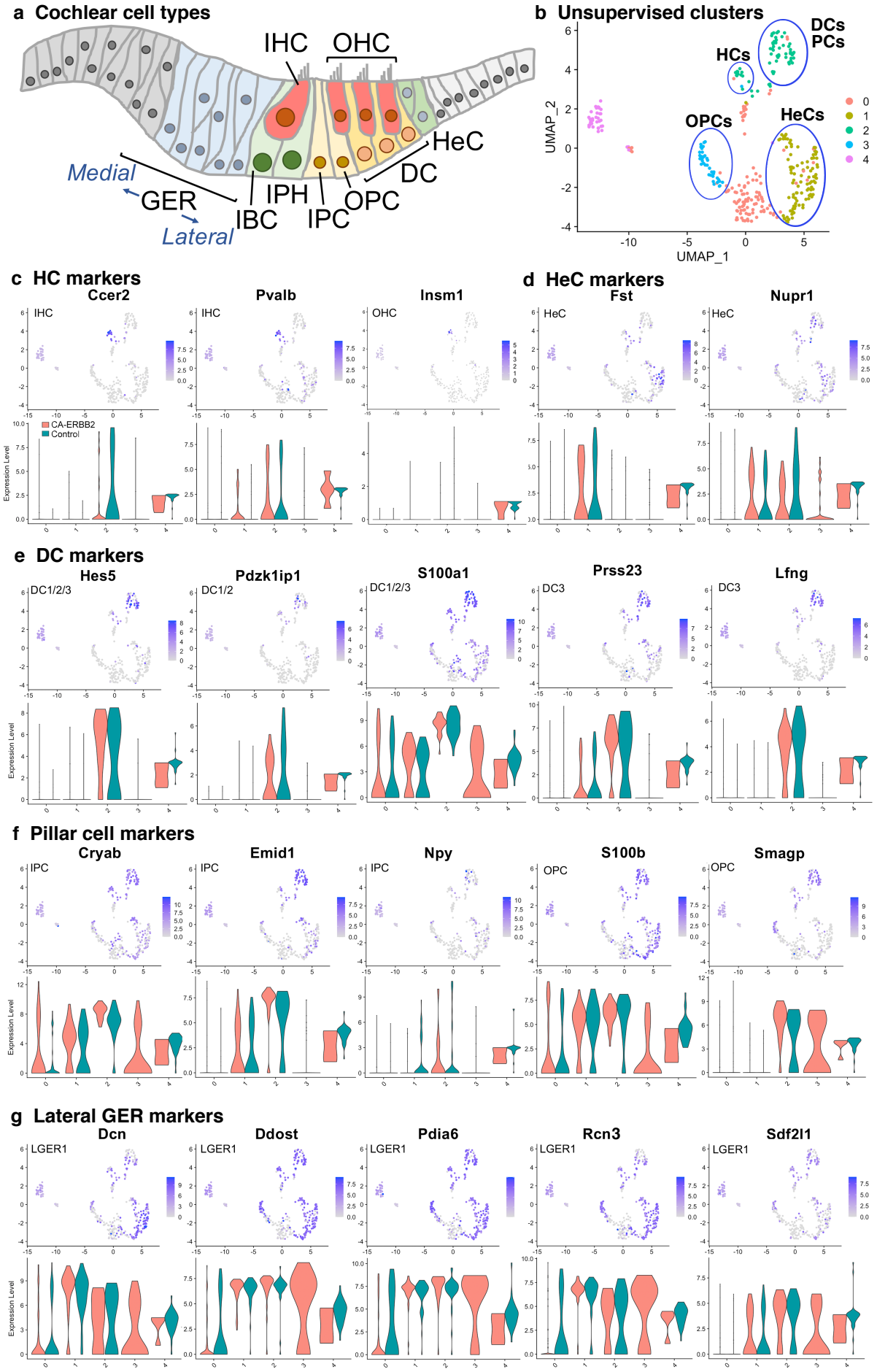
a Cochlear cell types
IHC
OHC
HeC
DC
OPC
IPC
IPH
IBC
GER
Medial
Lateral
b Unsupervised clusters
DCs
PCs
HCs
OPCs
HeCs
UMAP_2
UMAP_1
0
1
2
3
4
c HC markers
Ccer2
Pvalb
Insm1
IHC
OHC
CA-ERBB2
Control
Expression Level
d HeC markers
Fst
Nupr1
HeC
e DC markers
Hes5
Pdzk1ip1
S100a1
Prss23
Lfng
DC1/2/3
DC1/2
DC3
f Pillar cell markers
Cryab
Emid1
Npy
S100b
Smagp
IPC
OPC
g Lateral GER markers
Dcn
Ddost
Pdia6
Rcn3
Sdf2l1
LGER1

Figure 3

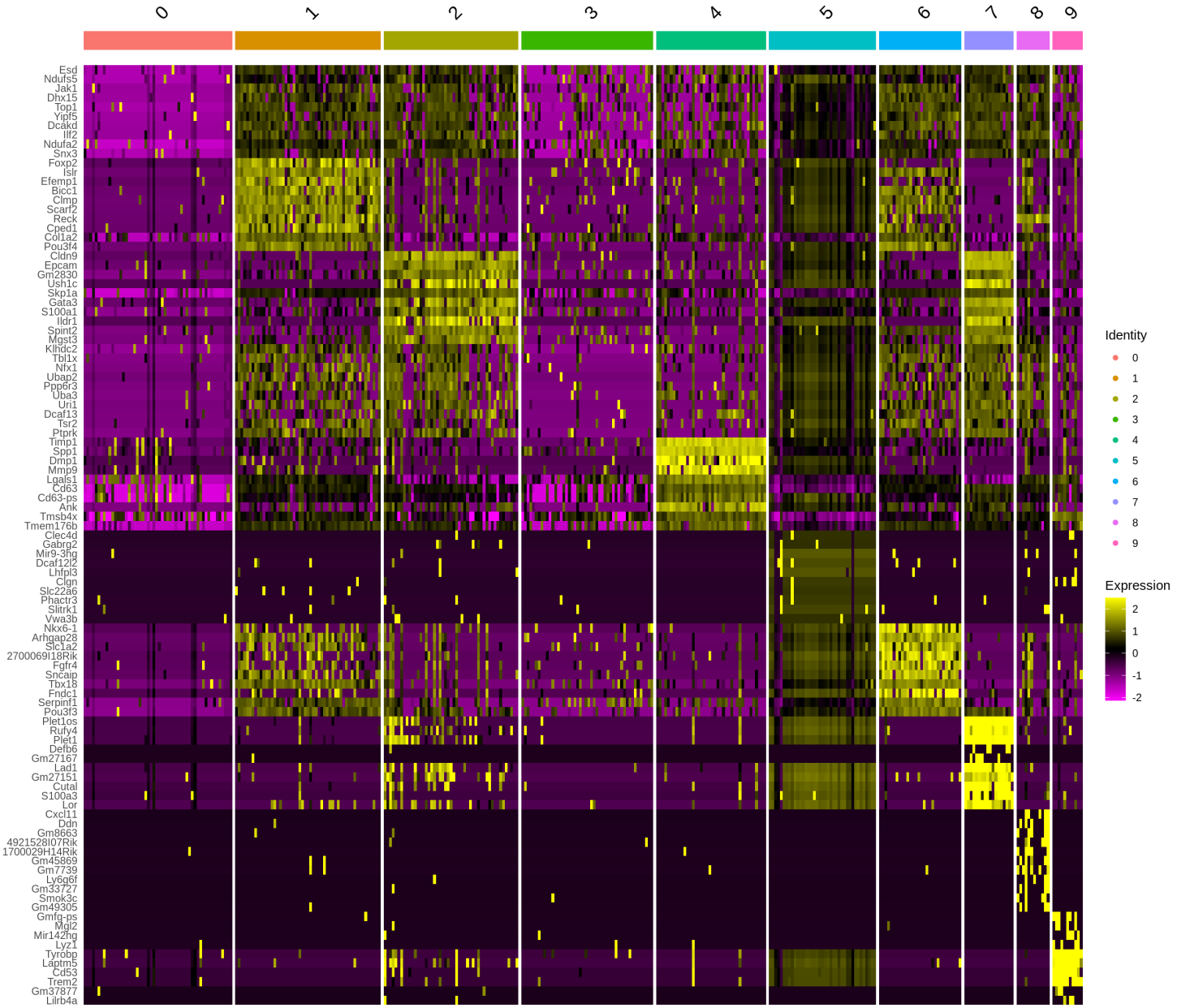
0
1
2
3
4
5
6
7
8
9
Esd
Ndufs5
Jak1
Dhx15
Top1
Yipf5
Dcakd
Ilf2
Ndufa2
Snx3
Foxp2
Islr
Efemp1
Bicc1
Clmp
Scarf2
Reck
Cped1
Col1a2
Pou3f4
Cldn9
Epcam
Gm2830
Ush1c
Skp1a
Gata3
S100a1
Ildr1
Spint2
Mgst3
Klhdc2
Tbl1x
Nfx1
Ubap2
Ppp6r3
Uba3
Uri1
Dcaf13
Tsr2
Ptprk
Timp1
Spp1
Dmp1
Mmp9
Lgals1
Cd63
Cd63-ps
Ank
Tmsb4x
Tmem176b
Clec4d
Gabrg2
Mir9-3hg
Dcaf12l2
Lhfpl3
Clgn
Slc22a6
Phactr3
Slitrk1
Vwa3b
Nkx6-1
Arhgap28
Slc1a2
2700069I18Rik
Fgfr4
Sncaip
Tbx18
Fndc1
Serpinf1
Pou3f3
Plet1os
Rufy4
Plet1
Defb6
Gm27167
Lad1
Gm27151
Cutal
S100a3
Lor
Cxcl11
Ddn
Gm8663
4921528I07Rik
1700029H14Rik
Gm45869
Gm7739
Ly6g6f
Gm33727
Smok3c
Gm49305
Gmfg-ps
Mdl2
Mir142hg
Lyz1
Tyrobp
Laptm5
Cd53
Trem2
Gm37877
Lilrb4a
Identity
0
1
2
3
4
5
6
7
8
9
Expression
2
1
0
-1
-2

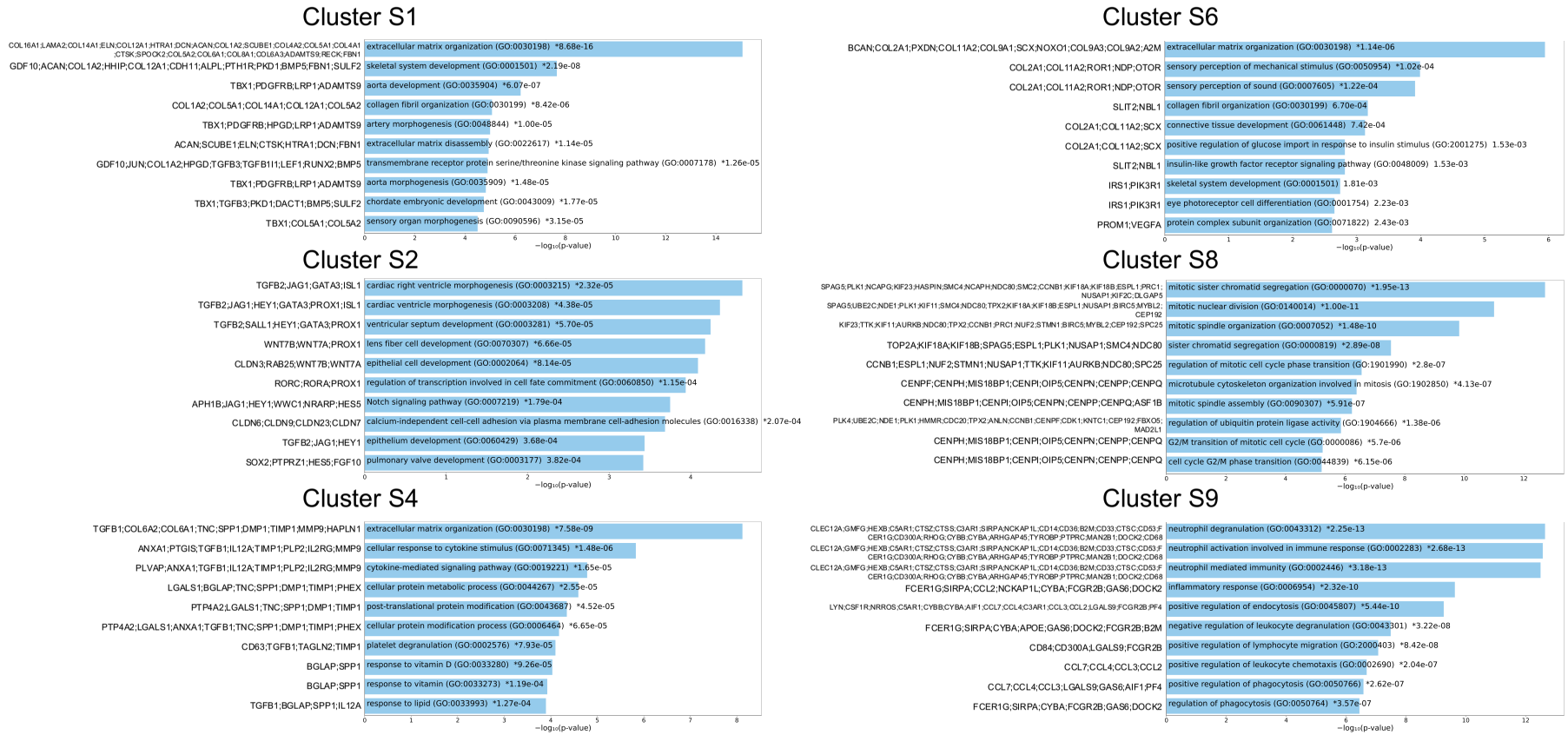
Cluster S1
COL16A1;LAMA2;COL14A1;ELN;COL12A1;HTRA1;DCN;ACAN;COL1A2;SCUBE1;COL4A2;COL5A1;COL4A1;CTSK;SPOCK2;COL5A2;COL6A1;COL8A1;COL6A3;ADAMTS9;RECK;FBN1 extracellular matrix organization (GO:0030198) *8.68e-16
GDF10;ACAN;COL1A2;HHIP;COL12A1;CDH11;ALPL;PTH1R;PKD1;BMP5;FBN1;SULF2 skeletal system development (GO:0001501) *2.19e-08
TBX1;PDGFRB;LRP1;ADAMTS9 aorta development (GO:0035904) *6.07e-07
COL1A2;COL5A1;COL14A1;COL12A1;COL5A2 collagen fibril organization (GO:0030199) *8.42e-06
TBX1;PDGFRB;HPGD;LRP1;ADAMTS9 artery morphogenesis (GO:0048844) *1.00e-05
ACAN;SCUBE1;ELN;CTSK;HTRA1;DCN;FBN1 extracellular matrix disassembly (GO:0022617) *1.14e-05
GDF10;JUN;COL1A2;HPGD;TGFB3;TGFB1I1;LEF1;RUNX2;BMP5 transmembrane receptor protein serine/threonine kinase signaling pathway (GO:0007178) *1.26e-05
TBX1;PDGFRB;LRP1;ADAMTS9 aorta morphogenesis (GO:0035909) *1.48e-05
TBX1;TGFB3;PKD1;DACT1;BMP5;SULF2 chordate embryonic development (GO:0043009) *1.77e-05
TBX1;COL5A1;COL5A2 sensory organ morphogenesis (GO:0090596) *3.15e-05
0 2 4 6 8 10 12 14
−log10(p-value)
Cluster S2
TGFB2;JAG1;GATA3;ISL1 cardiac right ventricle morphogenesis (GO:0003215) *2.32e-05
TGFB2;JAG1;HEY1;GATA3;PROX1;ISL1 cardiac ventricle morphogenesis (GO:0003208) *4.38e-05
TGFB2;SALL1;HEY1;GATA3;PROX1 ventricular septum development (GO:0003281) *5.70e-05
WNT7B;WNT7A;PROX1 lens fiber cell development (GO:0070307) *6.66e-05
CLDN3;RAB25;WNT7B;WNT7A epithelial cell development (GO:0002064) *8.14e-05
RORC;RORA;PROX1 regulation of transcription involved in cell fate commitment (GO:0060850) *1.15e-04
APH1B;JAG1;HEY1;WWC1;NRARP;HES5 Notch signaling pathway (GO:0007219) *1.79e-04
CLDN6;CLDN9;CLDN23;CLDN7 calcium-independent cell-cell adhesion via plasma membrane cell-adhesion molecules (GO:0016338) *2.07e-04
TGFB2;JAG1;HEY1 epithelium development (GO:0060429) 3.68e-04
SOX2;PTPRZ1;HES5;FGF10 pulmonary valve development (GO:0003177) 3.82e-04
0 1 2 3 4
−log10(p-value)
Cluster S4
TGFB1;COL6A2;COL6A1;TNC;SPP1;DMP1;TIMP1;MMP9;HAPLN1 extracellular matrix organization (GO:0030198) *7.58e-09
ANXA1;PTGIS;TGFB1;IL12A;TIMP1;PLP2;IL2RG;MMP9 cellular response to cytokine stimulus (GO:0071345) *1.48e-06
PLVAP;ANXA1;TGFB1;IL12A;TIMP1;PLP2;IL2RG;MMP9 cytokine-mediated signaling pathway (GO:0019221) *1.65e-05
LGALS1;BGLAP;TNC;SPP1;DMP1;TIMP1;PHEX cellular protein metabolic process (GO:0044267) *2.55e-05
PTP4A2;LGALS1;TNC;SPP1;DMP1;TIMP1 post-translational protein modification (GO:0043687) *4.52e-05
PTP4A2;LGALS1;ANXA1;TGFB1;TNC;SPP1;DMP1;TIMP1;PHEX cellular protein modification process (GO:0006464) *6.65e-05
CD63;TGFB1;TAGLN2;TIMP1 platelet degranulation (GO:0002576) *7.93e-05
BGLAP;SPP1 response to vitamin D (GO:0033280) *9.26e-05
BGLAP;SPP1 response to vitamin (GO:0033273) *1.19e-04
TGFB1;BGLAP;SPP1;IL12A response to lipid (GO:0033993) *1.27e-04
0 1 2 3 4 5 6 7 8
−log10(p-value)
Cluster S6
BCAN;COL2A1;PXDN;COL11A2;COL9A1;SCX;NOXO1;COL9A3;COL9A2;A2M extracellular matrix organization (GO:0030198) *1.14e-06
COL2A1;COL11A2;ROR1;NDP;OTOR sensory perception of mechanical stimulus (GO:0050954) *1.02e-04
COL2A1;COL11A2;ROR1;NDP;OTOR sensory perception of sound (GO:0007605) *1.22e-04
SLIT2;NBL1 collagen fibril organization (GO:0030199) 6.70e-04
COL2A1;COL11A2;SCX connective tissue development (GO:0061448) 7.42e-04
COL2A1;COL11A2;SCX positive regulation of glucose import in response to insulin stimulus (GO:2001275) 1.53e-03
SLIT2;NBL1 insulin-like growth factor receptor signaling pathway (GO:0048009) 1.53e-03
IRS1;PIK3R1 skeletal system development (GO:0001501) 1.81e-03
IRS1;PIK3R1 eye photoreceptor cell differentiation (GO:0001754) 2.23e-03
PROM1;VEGFA protein complex subunit organization (GO:0071822) 2.43e-03
0 1 2 3 4 5 6
−log10(p-value)
Cluster S8
SPAG5;PLK1;NCAPG;KIF23;HASPIN;SMC4;NCAPH;NDC80;SMC2;CCNB1;KIF18A;KIF18B;ESPL1;PRC1;NUSAP1;KIF2C;DLGAP5 mitotic sister chromatid segregation (GO:0000070) *1.95e-13
SPAG5;UBE2C;NDE1;PLK1;KIF11;SMC4;NDC80;TPX2;KIF18A;KIF18B;ESPL1;NUSAP1;BIRC5;MYBL2;CEP192 mitotic nuclear division (GO:0140014) *1.00e-11
KIF23;TTK;KIF11;AURKB;NDC80;TPX2;CCNB1;PRC1;NUF2;STMN1;BIRC5;MYBL2;CEP192;SPC25 mitotic spindle organization (GO:0007052) *1.48e-10
TOP2A;KIF18A;KIF18B;SPAG5;ESPL1;PLK1;NUSAP1;SMC4;NDC80 sister chromatid segregation (GO:0000819) *2.89e-08
CCNB1;ESPL1;NUF2;STMN1;NUSAP1;TTK;KIF11;AURKB;NDC80;SPC25 regulation of mitotic cell cycle phase transition (GO:1901990) *2.8e-07
CENPF;CENPH;MIS18BP1;CENPI;OIP5;CENPN;CENPP;CENPQ microtubule cytoskeleton organization involved in mitosis (GO:1902850) *4.13e-07
CENPH;MIS18BP1;CENPI;OIP5;CENPN;CENPP;CENPQ;ASF1B mitotic spindle assembly (GO:0090307) *5.91e-07
PLK4;UBE2C;NDE1;PLK1;HMMR;CDC20;TPX2;ANLN;CCNB1;CENPF;CDK1;KNTC1;CEP192;FBXO5;MAD2L1 regulation of ubiquitin protein ligase activity (GO:1904666) *1.38e-06
CENPH;MIS18BP1;CENPI;OIP5;CENPN;CENPP;CENPQ G2/M transition of mitotic cell cycle (GO:0000086) *5.7e-06
CENPH;MIS18BP1;CENPI;OIP5;CENPN;CENPP;CENPQ cell cycle G2/M phase transition (GO:0044839) *6.15e-06
0 2 4 6 8 10 12
−log10(p-value)
Cluster S9
CLEC12A;GMFG;HEXB;C5AR1;CTSZ;CTSS;C3AR1;SIRPA;NCKAP1L;CD14;CD36;B2M;CD33;CTSC;CD53;FCER1G;CD300A;RHOG;CYBB;CYBA;ARHGAP45;TYROBP;PTPRC;MAN2B1;DOCK2;CD68 neutrophil degranulation (GO:0043312) *2.25e-13
CLEC12A;GMFG;HEXB;C5AR1;CTSZ;CTSS;C3AR1;SIRPA;NCKAP1L;CD14;CD36;B2M;CD33;CTSC;CD53;FCER1G;CD300A;RHOG;CYBB;CYBA;ARHGAP45;TYROBP;PTPRC;MAN2B1;DOCK2;CD68 neutrophil activation involved in immune response (GO:0002283) *2.68e-13
CLEC12A;GMFG;HEXB;C5AR1;CTSZ;CTSS;C3AR1;SIRPA;NCKAP1L;CD14;CD36;B2M;CD33;CTSC;CD53;FCER1G;CD300A;RHOG;CYBB;CYBA;ARHGAP45;TYROBP;PTPRC;MAN2B1;DOCK2;CD68 neutrophil mediated immunity (GO:0002446) *3.18e-13
FCER1G;SIRPA;CCL2;NCKAP1L;CYBA;FCGR2B;GAS6;DOCK2 inflammatory response (GO:0006954) *2.32e-10
LYN;CSF1R;NRROS;C5AR1;CYBB;CYBA;AIF1;CCL7;CCL4;C3AR1;CCL3;CCL2;LGALS9;FCGR2B;PF4 positive regulation of endocytosis (GO:0045807) *5.44e-10
FCER1G;SIRPA;CYBA;APOE;GAS6;DOCK2;FCGR2B;B2M negative regulation of leukocyte degranulation (GO:0043301) *3.22e-08
CD84;CD300A;LGALS9;FCGR2B positive regulation of lymphocyte migration (GO:2000403) *8.42e-08
CCL7;CCL4;CCL3;CCL2 positive regulation of leukocyte chemotaxis (GO:0002690) *2.04e-07
CCL7;CCL4;CCL3;LGALS9;GAS6;AIF1;PF4 positive regulation of phagocytosis (GO:0050766) *2.62e-07
FCER1G;SIRPA;CYBA;FCGR2B;GAS6;DOCK2 regulation of phagocytosis (GO:0050764) *3.57e-07
0 2 4 6 8 10 12
−log10(p-value)

Figure 4

Figure 5

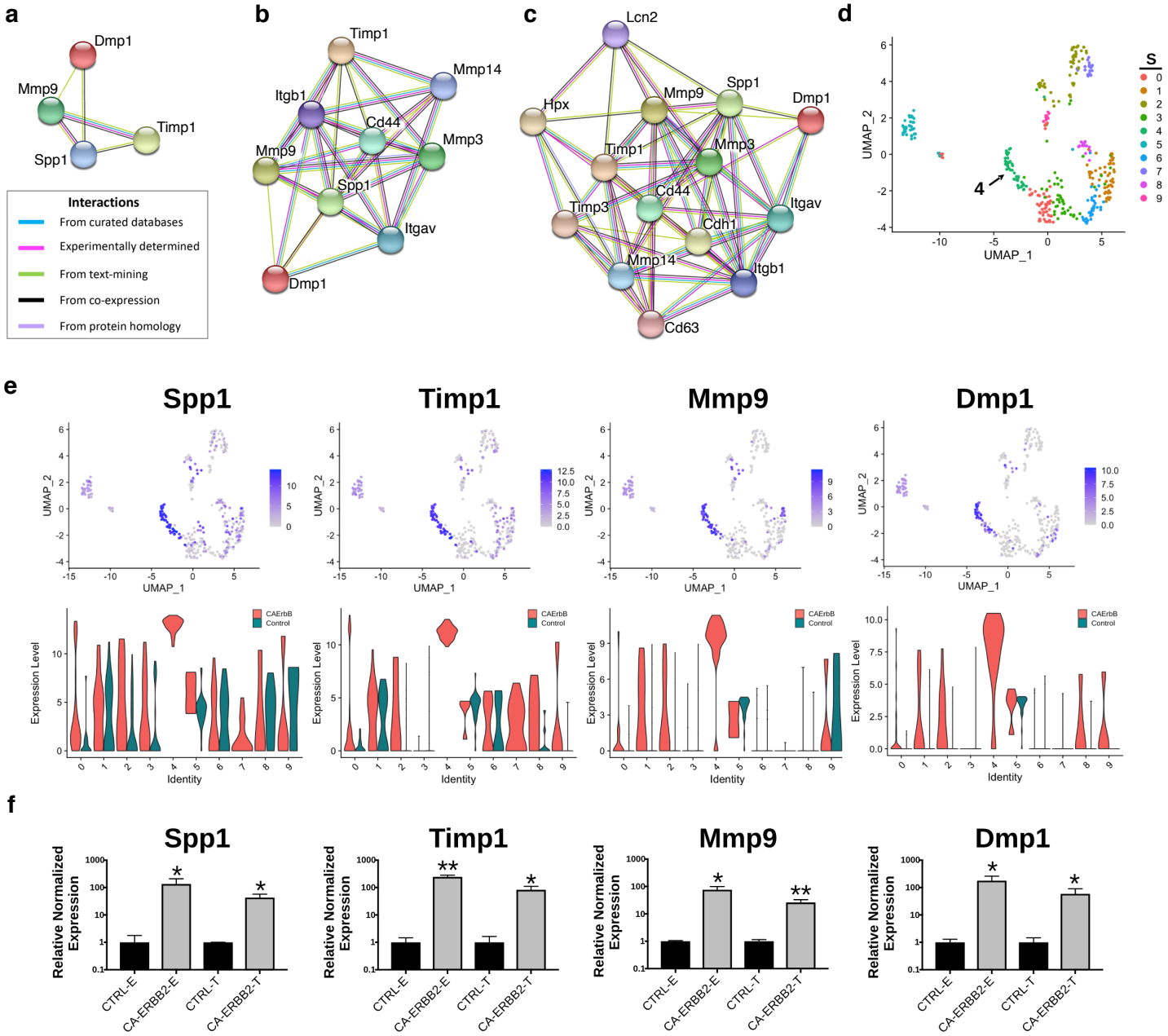
a
Dmp1
Mmp9
Timp1
Spp1
Interactions
From curated databases
Experimentally determined
From text-mining
From co-expression
From protein homology
b
Timp1
Mmp14
Itgb1
Cd44
Mmp3
Mmp9
Spp1
Itgav
Dmp1
c
Lcn2
Hpx
Mmp9
Spp1
Dmp1
Timp1
Mmp3
Cd44
Timp3
Itgav
Cdh1
Mmp14
Itgb1
Cd63
d
UMAP_2
UMAP_1
4
S
0
1
2
3
4
5
6
7
8
9
e
Spp1
Timp1
Mmp9
Dmp1
UMAP_2
UMAP_1
CAErbB
Control
Expression Level
Identity
f
Spp1
Timp1
Mmp9
Dmp1
Relative Normalized Expression
CTRL-E
CA-ERBB2-E
CTRL-T
CA-ERBB2-T

Figure 6

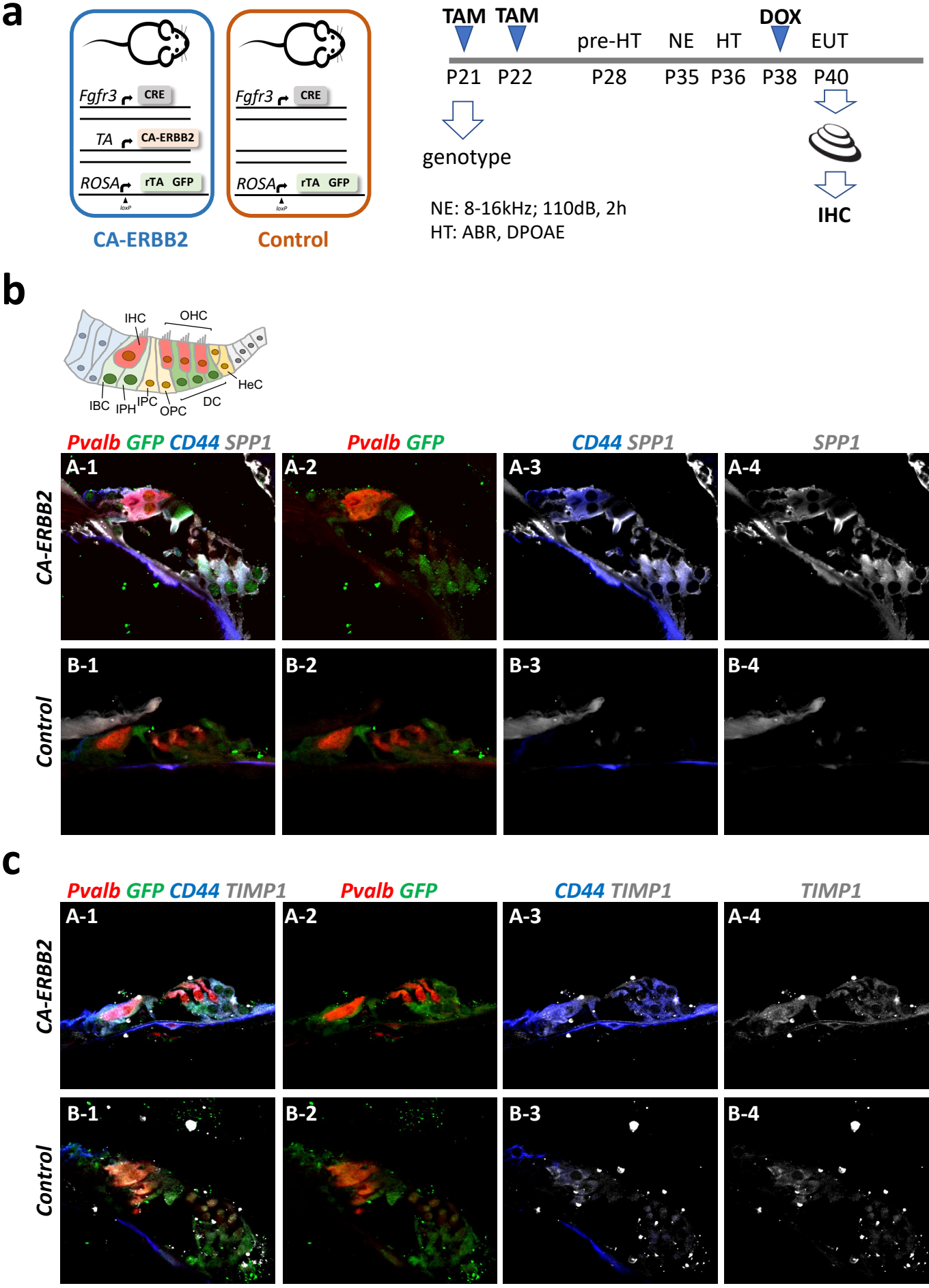
a
Fgfr3
CRE
TA
CA-ERBB2
ROSA
rTA GFP
loxP
CA-ERBB2
Control
TAM TAM
DOX
pre-HT NE HT EUT
P21 P22 P28 P35 P36 P38 P40
genotype
IHC
NE: 8-16kHz; 110dB, 2h
HT: ABR, DPOAE
b
IHC
OHC
HeC
IBC IPH IPC OPC DC
Pvalb GFP CD44 SPP1
Pvalb GFP
CD44 SPP1
SPP1
CA-ERBB2
Control
A-1
A-2
A-3
A-4
B-1
B-2
B-3
B-4
c
Pvalb GFP CD44 TIMP1
Pvalb GFP
CD44 TIMP1
TIMP1
CA-ERBB2
Control
A-1
A-2
A-3
A-4
B-1
B-2
B-3
B-4

Figure 7

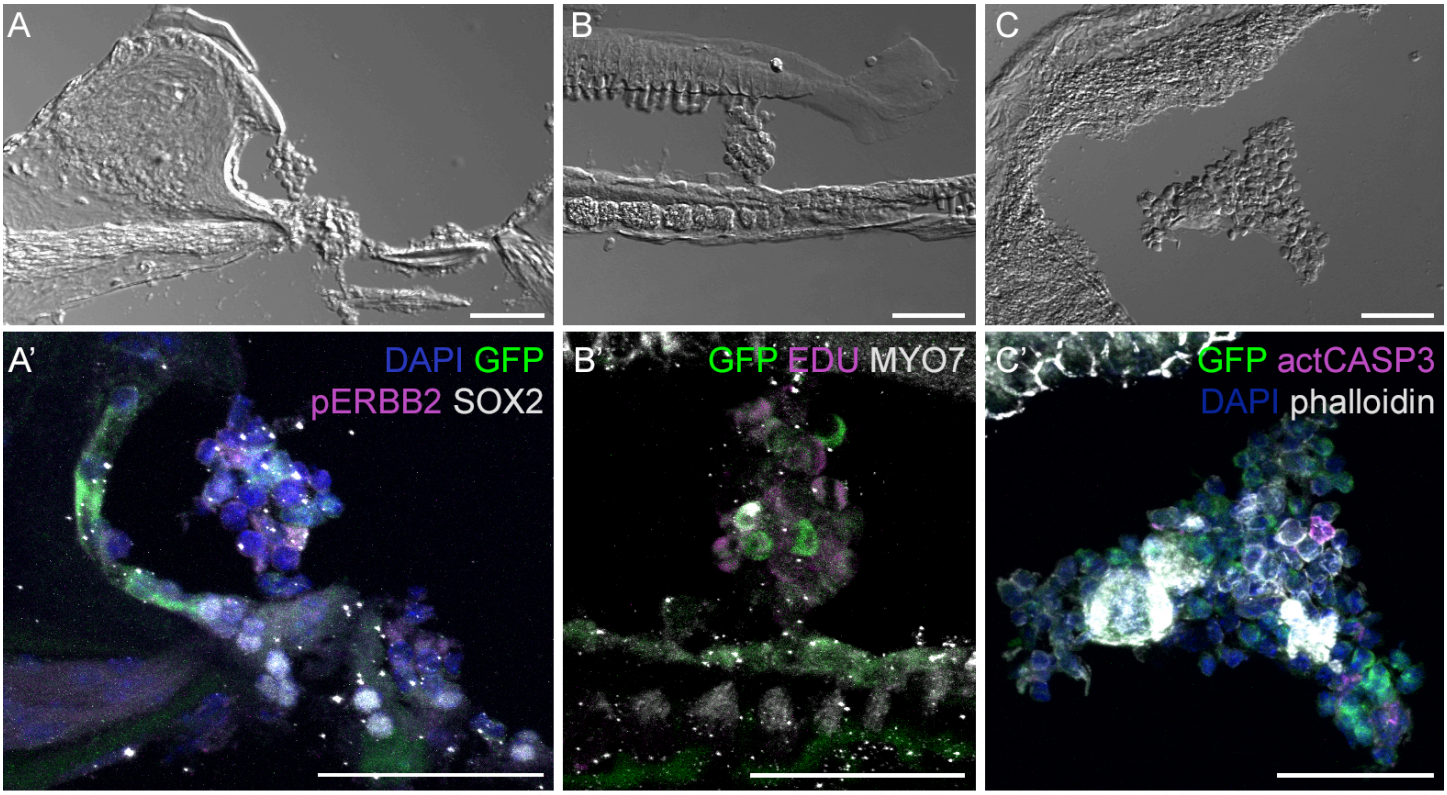
A
B
C
A'
DAPI GFP
pERBB2 SOX2
B'
GFP EDU MYO7
C'
GFP actCASP3
DAPI phalloidin

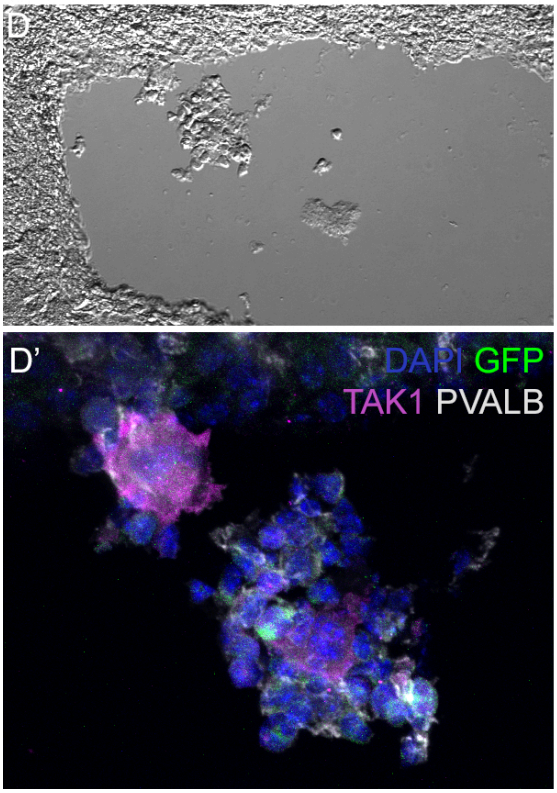
D
D'
DAPI GFP
TAK1 PVALB